Ecology, 89(2), 2008, pp. 353–362

EFFECTS OF CLIMATE CHANGE ON PHENOLOGY, FROST DAMAGE, AND FLORAL ABUNDANCE OF MONTANE WILDFLOWERS

David W. Inouye[1,2,3]

[1]*Department of Biology, University of Maryland, College Park, Maryland 20742-4415 USA*
[2]*Rocky Mountain Biological Laboratory, P.O. Box 519, Crested Butte, Colorado 81224 USA*

Abstract. The timing of life history traits is central to lifetime fitness and nowhere is this more evident or well studied as in the phenology of flowering in governing plant reproductive success. Recent changes in the timing of environmental events attributable to climate change, such as the date of snowmelt at high altitudes, which initiates the growing season, have had important repercussions for some common perennial herbaceous wildflower species. The phenology of flowering at the Rocky Mountain Biological Laboratory (Colorado, USA) is strongly influenced by date of snowmelt, which makes this site ideal for examining phenological responses to climate change. Flower buds of *Delphinium barbeyi*, *Erigeron speciosus*, and *Helianthella quinquenervis* are sensitive to frost, and the earlier beginning of the growing season in recent years has exposed them to more frequent mid-June frost kills. From 1992 to 1998, on average 36.1% of *Helianthella* buds were frosted, but for 1999–2006 the mean is 73.9%; in only one year since 1998 have plants escaped all frost damage. For all three of these perennial species, there is a significant relationship between the date of snowmelt and the abundance of flowering that summer. Greater snowpack results in later snowmelt, later beginning of the growing season, and less frost mortality of buds. Microhabitat differences in snow accumulation, snowmelt patterns, and cold air drainage during frost events can be significant; an elevation difference of only 12 m between two plots resulted in a temperature difference of almost 2°C in 2006 and a difference of 37% in frost damage to buds. The loss of flowers and therefore seeds can reduce recruitment in these plant populations, and affect pollinators, herbivores, and seed predators that previously relied on them. Other plant species in this environment are similarly susceptible to frost damage so the negative effects for recruitment and for consumers dependent on flowers and seeds could be widespread. These findings point out the paradox of increased frost damage in the face of global warming, provide important insights into the adaptive significance of phenology, and have general implications for flowering plants throughout the region and anywhere climate change is having similar impacts.

Key words: *climate change;* Delphinium barbeyi; Erigeron speciosus; *flowering; frost; growing season;* Helianthella quinquenervis; *phenology; Rocky Mountain Biological Laboratory; snowmelt, subalpine.*

Introduction

The phenology of reproduction is an important life history trait that influences fitness in a variety of ways. Reproducing at the wrong time, in advance of or after the appropriate season, may lead to failure in finding mates, failure to match demands of growing offspring with temporal peaks in food resources (e.g., Visser et al. 1998), or failure by a pollinator to find pollen and nectar, or failure of a flower to be pollinated. Given these potentially severe consequences, it is not surprising that in many cases the phenology of reproduction has evolved to rely on environmental cues that have proven to be reliable indicators of appropriate timing of reproductive effort. An ecological and evolutionary dilemma is posed to a variety of organisms now because of the environmental changes accompanying global climate change. Can they respond in appropriate ways to these ongoing changes so that their phenology remains synchronous with other species with which they interact? And can they adjust their responses to previously reliable environmental cues for timing of reproduction? These questions are difficult to answer without long-term observations and experiments.

The phenology of flowering by herbaceous wildflowers at high altitudes where there is significant snowfall is primarily a consequence of one environmental event, the disappearance of the snowpack (Inouye and Wielgolaski 2003). This event is in turn influenced by a variety of factors, including global, regional, and local climate. Global influences include ongoing changes in temperature and precipitation regimes, with high-altitude environments warming and receiving more precipitation as rain instead of snow (Beniston and Fox 1996, Johnson 1998). Regional influences on snowpack in the western United States include the El Niño/Southern Oscillation

Manuscript received 22 December 2006; revised 7 May 2007; accepted 22 May 2007. Corresponding Editor: S. Naeem. For reprints of this Special Feature, see footnote 1, p. 319.
[3] E-mail: Inouye@umd.edu

TABLE 1. Study species.

Species (family)	Common name	Average flowering dates	Units counted
Delphinium barbeyi (Ranunculaceae)	subalpine larkspur	mid-July	flowers and inflorescences
Helianthella quinquenervis (Asteraceae)	aspen sunflower	mid to late July	capitulae and inflorescences
Erigeron speciosus (Asteraceae)	aspen fleabane	late July	capitulae

(ENSO; Diaz et al. 2003) and the North Pacific Oscillation (Pacific Decadal Oscillation; Grissino-Mayer et al. 2004). Local influences include topographic variables such as slope and aspect, which affect the accumulation and melting of snowpack (Miller 1982, Kudo and Hirao 2006), and the occurrence of cold air drainage that creates thermal and phenological inversions (Lynov 1984). At present, the net result of these environmental changes seems to be a trend toward earlier snowmelt, and hence earlier arrival of spring in the western United States (Cayan et al. 2001) and other mountain areas (Dankers and Christensen 2005). The phenology of high latitudes may show many of the same characteristics that high altitudes do (Wielgolaski and Inouye 2003).

Earlier beginning of the growing season due to earlier snowmelt can have multiple consequences. It could increase the length of the photosynthetic period, if the end of the season remains fixed or changes to a later date. If drought is a problem at the end of the growing season, however, earlier snowmelt and longer snow-free periods may increase exposure of plants to this stress (Giménez-Benavides et al. 2007). Earlier snowmelt can significantly alter the dates on which species may come into bloom throughout the summer (Inouye and McGuire 1991, Inouye et al. 2002, 2003, Saavedra et al. 2003) because the ground and air will warm up when the snow disappears. For some species there may also be a correlation between timing of snowmelt and the abundance of flowering (e.g., *Delphinium* species [Inouye et al. 2002, Saavedra et al. 2003]).

One of the factors linking dates of snowmelt to flowering abundance is frost (Inouye 2000, Inouye et al. 2002). If the probability of spring frost on a particular calendar date remains fixed, but leaf or flower buds are being initiated at earlier dates and thus are more vulnerable when frosts occur, the frequency of frost damage to frost-sensitive species is expected to increase. Frost damage might also increase even if the date of last spring frost is becoming later, if the rate of change in frost dates is slower than that of change in snowmelt dates.

In this study, I report data for three species of high-altitude herbaceous wildflowers that have flower buds susceptible to frost damage (Table 1). All three of these long-lived perennials can experience total mortality of flower buds due to late spring frost events. The availability of a long-term data set on flowering phenology is used to look for evidence in the past few decades of changes suggested above in the timing of snowmelt relative to flowering, and possible influences on timing and abundance of flowering.

METHODS

Study site.—An ongoing long-term study of flowering phenology is being conducted at the Rocky Mountain Biological Laboratory (RMBL), in the Colorado Rocky Mountains (38°57′ N, 106°59′ W). RMBL is located at 2886 m elevation in the East River valley of the West Elk Mountains, approximately 9.5 km north of the town of Crested Butte, Colorado, USA. In 1973, several sets of 2 × 2 m plots were established by a group of researchers at RMBL for monitoring flowering phenology. For a separate study, two larger plots were established (1974 and 1975) to monitor abundance of flowering by *Helianthella quinquenervis*.

Focal species.—This study reports on data for *Delphinium barbeyi* and *Erigeron speciosus* (see Plate 1) from two subsets of the total of 30 phenology plots, one set in a mesic meadow on level ground (altitudes 2864–2870 m) adjacent to the junction of the East River and Copper Creek (originally established and monitored by Graham Pyke) and the other on dry rocky meadows at slightly higher elevations (2927–2970 m), along the Copper Creek trail and the portion of Forest Service trail #401 that crosses RMBL property. Data on flower abundance for *Helianthella quinquenervis* have been collected each year since 1974 from one plot (lower plot, 10 × 45 m; mean altitude about 2893 m) or 1975 for a second plot (upper plot, 10 × 36.5 m; mean altitude about 2905 m). GPS coordinates for the two plots, located above and below the Copper Creek trail in the Gothic town site, are available at the RMBL web site, and a map is presented in Fig. 1.

Empirical design.—Every other day for most or all of the growing season, all flowers in the 2 × 2 m phenology plots are counted, typically as number per inflorescence or ramet. A map, GPS coordinates for plot corners, and altitudes for the individual plots are available at the RMBL web site (*available online*).[4] For *Helianthella*, the number of flowers per stalk is counted on all inflorescences in each plot annually in July, and the number of inflorescences cut or broken off, and those with missing flowers (typically due to herbivory by deer or pocket gophers), is also counted. Since 1989, the annual mean number of flowers per stalk has been used to estimate the number of missing flowers (typically fewer than 1% of stalks were cut and/or missing flowers), to calculate a

[4] ⟨www.rmbl.org⟩

total number of flowers produced in each plot. Each year since 1994, counts have also been made of the number of frost-killed inflorescences. The inflorescences are typically developed enough to identify frost-killed ones easily (a stalk starts developing instead of just petioles on a vegetative rosette).

Environmental measurements.—Snowmelt data are from daily observations by billy barr of snowpack at a measurement station at the north edge of the RMBL, within 1 km of the plots. Temperature data are from the Crested Butte NOAA weather station.

Analytical methods.—Data for each phenology plot in each year are stored in individual spreadsheets. Statistical analyses were accomplished using SigmaPlot (Systat Software, San Jose, California, USA).

Results

The initiation of the flowering season at this study site is highly variable. Data from three additional species from the phenology plots that represent two of the earliest species and the latest to flower illustrate this, and help to set the context for variation and patterns shown by the three focal species. The first flowers each spring are typically *Claytonia lanceolata* (Portulacaceae), which bloom within a few days after snow melts; its first flowering dates have been as early as 14 April (2002) and as late as 9 June (1995) in the same 2×2 m plot (Rocky Meadow #7). The correlation between date of snowmelt and first flowering date is highly significant for species that flower early (e.g., for *Delphinium nuttallianum*, $r^2 = 0.734$, $P < 0.0001$; data for seven plots, 1975–2006, 1990 missing, mean flowering date 11 June, range 27 May–2 July) and late (e.g., for *Artemisia tridentata* [sagebrush], $r^2 = 0.600$, $P = 0.0001$; data only available from one plot, 1975–2006, 1989–1990 missing, mean flowering date 14 August, range 29 July–30 August).

Delphinium barbeyi

This species flowered in 3–12 plots/yr (mean 8.8; including frost-killed buds as years with flowering) between 1973 and 2006 (data were only collected on first flowering and not peak flowering for 1976, and no data were collected in 1990); non-flowering plants were present in most of the 12 plots in most years, but in some years most or all flower buds on plants that developed inflorescences were killed by frost, reducing the sample size for flowering dates. The average number of years (out of 32) that each plot had flowers was 25.2 (range 14–32). The earliest annual average for flowering (the first flower in all plots with flowers) was 1 July (day of year 182.7, in 2006; $n = 6$ plots) and the latest was 5 August (day of year 217.7, in 1995; $n = 10$ plots). The mean date of first flower (mean of annual means) was 14 July (day of year 195.7; median 15 July). For years with early snowmelt (before 19 May, day 139), there is no significant correlation between flowering date and snowmelt date (mean flowering date = day 189, 8 July), but for years with later snowmelt there is a significant correlation between these variables ($r^2 = 0.745$, $P < 0.0001$; Fig. 2). This split in the data set (made by visual inspection of the data) makes sense biologically as it indicates that there is a threshold effect between snowpack melt date and timing of flowering. This effect could be mediated by a requirement to accumulate a certain number of degree days before flowering occurs, with it taking longer to accumulate that heat sum in years with early snowmelt.

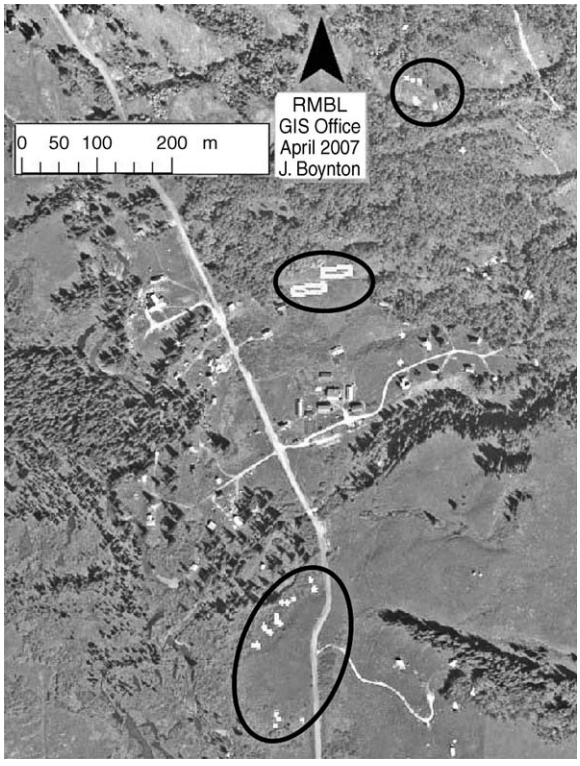

Fig. 1. Aerial view of the Rocky Mountain Biological Laboratory. The vertical road is Gunnison County Road 317, and north is indicated by the arrowhead. The plots used for *Delphinium barbeyi* and *Erigeron speciosus* are included in the upper and lower ellipses, and the *Helianthella quinquenervis* plots are the two larger plots in the middle ellipse.

As was reported in Inouye et al. (2002), there is a significant correlation between winter snowpack and the abundance of flowering for *Delphinium barbeyi*. Fig. 3 shows this relationship, using snowpack remaining on 30 April and including the seven additional years of data collected since that paper appeared; data for peak flowering were incomplete for 1973–1976. One plot (Veratrum Removal #1) had an unusually large number of flowers in 2004, causing that year to appear as an outlier.

Erigeron speciosus

This species is found in both dry, rocky meadow plots ($n = 7$ plots) and wet meadow plots ($n = 9$ plots), and because these tend to melt out at different times (rocky meadow plots are earlier) some correlations are shown

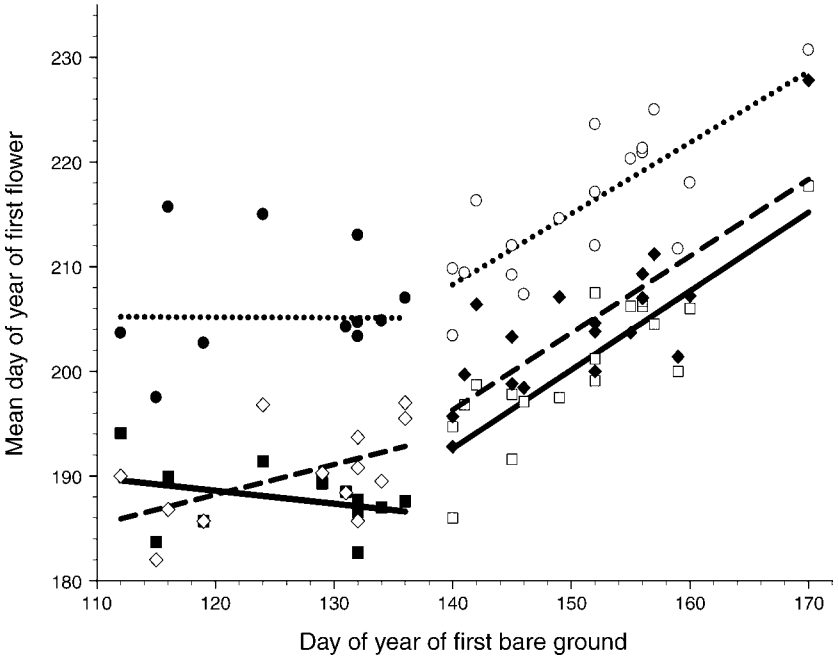

FIG. 2. The relationship between mean day of year of the first flowers of *Delphinium barbeyi* and *Erigeron speciosus* in the phenology plots and the day of year of first bare ground. The data were broken into two subsets by visual inspection; the early set (through day 139) has no significant slope or correlation for either species, and both are significant for the later set ($r^2 = 0.745$, $P < 0.0001$, $N = 18$ years). *Delphinium* data are shown with squares (solid for 12 early years, open for late years), and solid lines indicate the best fits. Data for *Erigeron* are shown separately for the seven dry, rocky, meadow plots (diamonds, open for 13 early years, solid for 18 late years) and nine wet meadow plots (circles; solid for early years and open for late years). For *Erigeron speciosus*, the equation for the later snowmelt dates for rocky meadow plots is $y = 0.734x + 93.506$ (dashed line, $r^2 = 0.629$, $P < 0.0001$); the equation for later snowmelt dates for wet meadow plots is $y = 0.679x + 113.223$ (dotted line, $r^2 = 0.620$, $P < 0.0001$).

separately for each habitat (Fig. 2). *Erigeron* flowered in 6–15 plots/yr (mean 11.0) between 1973 and 2006 (missing data for rocky meadow plots for 1976 and for both habitats in 1990); non-flowering plants were present in most of these plots in most years, but in some years most or all flower buds were killed by frost, reducing the sample size for flowering dates. The average number of years (out of 30) that these 15 plots

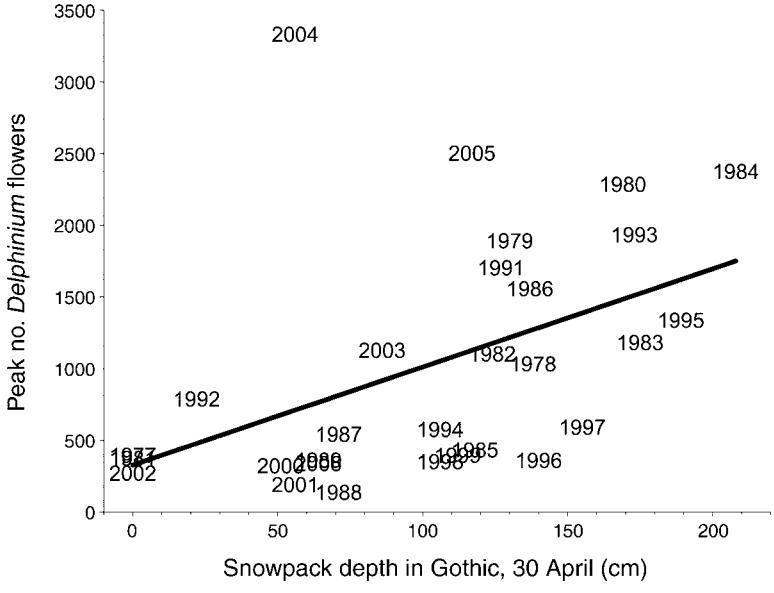

FIG. 3. The relationship between peak abundance of *Delphinium barbeyi* flowers and the amount of snow left on the ground on 30 April of that year ($y = 6.85x + 326.83$, $r^2 = 0.217$, $P = 0.011$, $N = 29$ years).

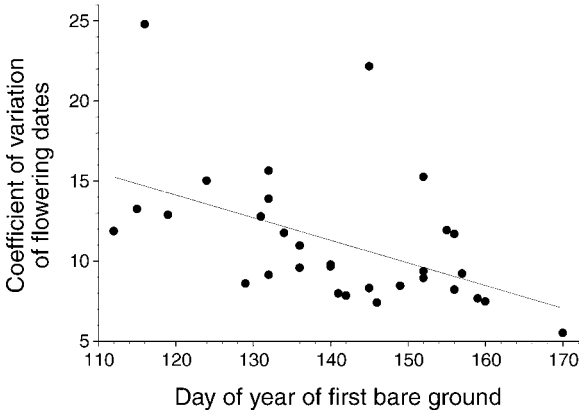

FIG. 4. The relationship between variability of flowering date of *Erigeron speciosus* and the date of snowmelt. Coefficient of variation is calculated using data from both habitats (dry and wet meadow.

had flowers was 22.3 (range 1–30). The earliest annual average for flowering (the first flower in all plots with flowers) was 9 July (day of year 190.2, in 2004; $n = 9$ plots) and the latest was 17 August (day of year 229.3, in 1995, $n = 12$ plots). The mean date of first flower (mean of annual means) was 30 July (day of year 210.5; median 25 July), and annual dates of first flower are dependent on snowmelt date. For wet meadow plots, in years with early snowmelt (before 19 May, day 139, $n = 12$ plots), there is no significant correlation between flowering date and snowmelt date (mean flowering date = 205, 24 July), but for years with later snowmelt there is a significant correlation between these variables ($r^2 = 0.620$, $P < 0.0001$, $n = 18$ plots; Fig. 2). For rocky meadow plots, in years with early snowmelt there is no significant correlation between flowering date and snowmelt date (mean flowering date = 190, 9 July, $n = 13$ plots), but for years with later snowmelt there is a significant correlation between these variables ($r^2 = 0.629$, $P < 0.0001$, $n = 18$ plots; Fig. 2).

There is a significant correlation between the date of snowmelt and the coefficient of variation of flowering date ($r^2 = 0.247$, $P = 0.005$; Fig. 4), with earlier snowmelt correlating with increased variability in flowering date among plots. There is also a clear pattern between the first date of bare ground and the abundance of flowers the following summer. For years with early snowmelt (before 19 May, day 139), there is no significant correlation between number of flowers and snowmelt date (mean = 204 flowers), but for years with later snowmelt there is a trend between these variables ($r^2 = 0.131$, $P = 0.14$; Fig. 5). This split in the data set makes sense biologically as it indicates that there may be a threshold effect between date of snowmelt and frost damage. It appears that if snow melts out before 19 May (or there is less than a meter of snow left on the ground on 30 April) there is a strong likelihood of frost damage the following summer.

Helianthella quinquenervis

The number of flower heads of the aspen sunflower in the two plots combined has varied over four orders of magnitude from 1975 to 2006, ranging from 1 (2004) to 4448 (1982) (Fig. 6). Since 1992, when I first began quantifying frost damage, the percentage of flower buds

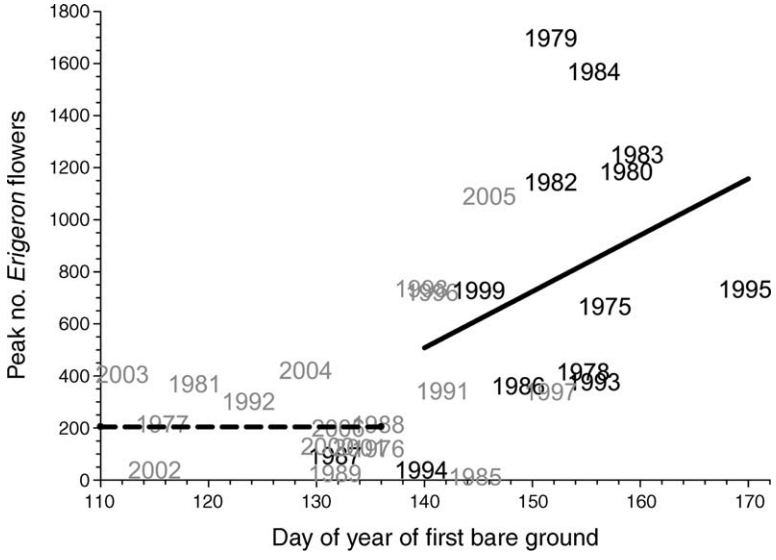

FIG. 5. The relationship between peak abundance of *Erigeron speciosus* flowers and the first date of bare ground of that year. The data were broken into two subsets by visual inspection; the early set (through day 139) has no significant slope or correlation. The dashed line indicates the mean number of flowers for years with snowmelt dates earlier than 19 May (day 139). The equation for the later snowmelt dates (solid line) is $y = 21.65x - 2523.30$, $r^2 = 0.131$, $P = 0.14$). The driest summer from 1925 to 2006 was 1994, and most flower buds dried up before opening. Years in gray are those in which I recorded evidence of frost damage in my field notes.

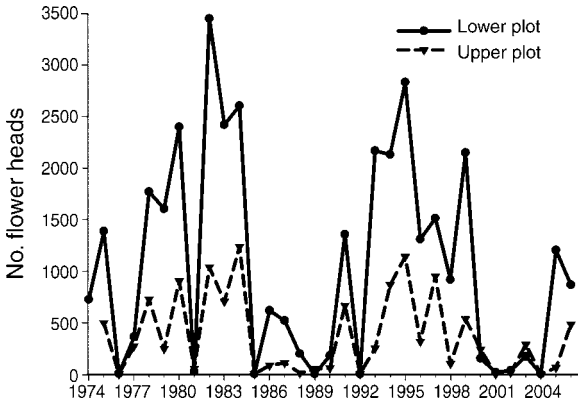

FIG. 6. The number of unfrosted *Helianthella quinquenervis* flower heads in two plots (lower plot, 450 m^2; upper plot, 365 m^2) at the Rocky Mountain Biological Laboratory, Colorado, USA. Years with very few flowers are typically years in which frost killed most flower buds.

killed by frost has ranged from 0% to 100% (Fig. 7). Over the past eight years, bud mortality has been zero in one year; in the other seven years it has ranged from 65% to 100%. The probability and degree of frost damage appears to be correlated with the previous winter's snowpack. For years with early snowmelt (before 19 May, day 139), there is no significant correlation between the number of unfrosted flower heads and snowmelt date, but for years with later snowmelt there is a significant correlation between these variables ($r^2 = 0.363$, $P = 0.008$; Fig. 8).

DISCUSSION

Collectively, these results provide evidence for significant and detrimental impacts of current climate trends on some subalpine flowers, mediated by their phenological responses to snowmelt. The impacts are variable among species, but are clearly related to life history, and have the potential to result in demographic changes in the populations due to lack of seed production. All three of the three focal wildflower species are long-lived perennials, with life spans that can probably reach multiple decades (estimates based on excavation of roots and tagging of individual *Helianthella* plants). This confers an element of stability to their presence in these plots, although there is evidence of turnover. For example, in one phenology plot (Willow-Meadow Interface #2) *Delphinium barbeyi* has only flowered in one year since 1988, and in another (Willow-Meadow Interface #5) it has not flowered since 1993 (although there were aborted flower stalks in 1994). It first appeared in *Veratrum* Removal Plot #1 in 1979 (possibly a consequence of the removal of *Veratrum tenuipetalum* (Melanthiaceae (Liliaceae)) beginning in 1974).

During this study, there has been an increase in the frequency of frost damage. For example, during the first 11 years of the *Helianthella* study (1974–1984) there were two years with significant frost damage (inferred as years with almost no flowers), while there have only been two years without significant frost damage in the past 11 years (Figs. 6 and 7). Biologically, it makes sense that there might be a threshold level of snow that will delay flower bud development beyond the time when frost is still likely to occur. The data reported in this paper are consistent with the interpretation that the likelihood and degree of frost damage to flower buds are strongly affected by snowmelt date.

Radiation frost (exposure to the cold night sky) alone does not seem to cause significant damage to flowers at

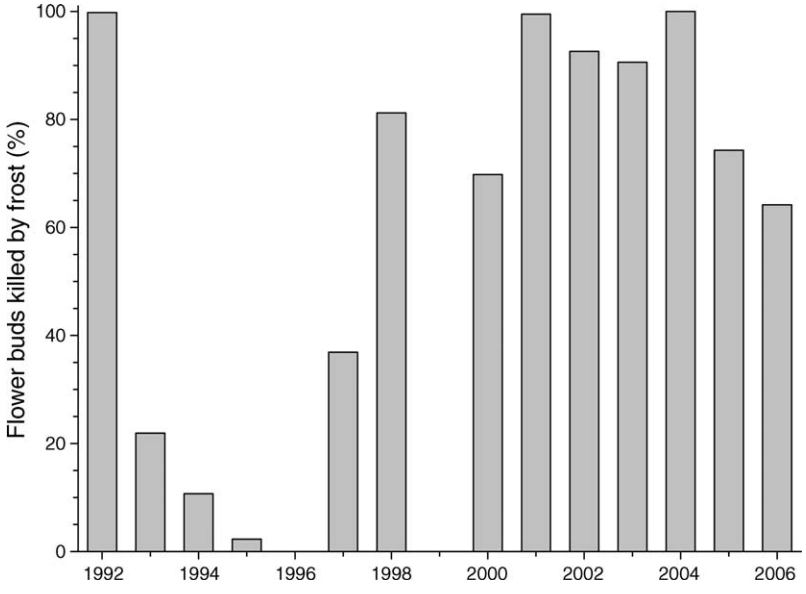

FIG. 7. The percentage of *Helianthella quinquenervis* flower buds that were killed by frost, 1992–2006. Data are from both plots (upper and lower) combined.

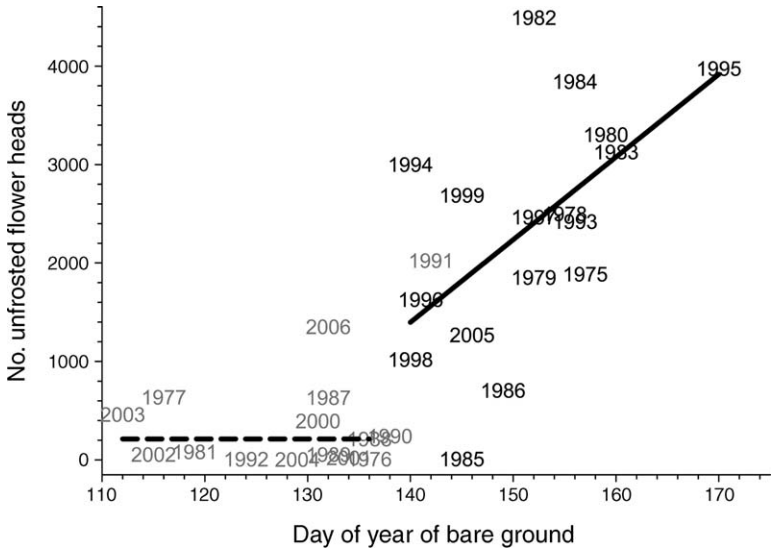

FIG. 8. The relationship between production of *Helianthella quinquenervis* flower heads that were not killed by frost in two plots and the first date of bare ground. The data were broken into two subsets by visual inspection; the early set (through day 139, in gray) has no significant slope or correlation, and both are significant for the later set ($r^2 = 0.313$, $P = 0.02$). The five partially overlapping early snowmelt data points are (counterclockwise from 2004) 1989, 2001, 1976, 1990, and 1988.

the study site; it is primarily convective frost (cold air masses) that affects them. The minimum temperature in June, when the frost damage occurs, has been trending ($r^2 = 0.077$, $P = 0.06$; data for the Crested Butte NOAA weather station, 1960–2005) toward lower temperatures; during the time of this study (1973–2005) the June minimum has averaged −4.3°C (range −1.7°C to −8.3°C). Unless this trend is reversed, potentially through global warming, frost damage is likely to continue to be a common event.

Several other species in my study site at RMBL are affected by spring frost that kills leaf buds, inflorescences, and developing fruits. For example, frost can damage new growth on Engelmann spruce (*Picea engelmannii*; Pinaceae) and subalpine fir (*Abies lasiocarpa*; Pinaceae), leaves of *Heracleum lanatum* (Apiaceae), fruits of *Erythronium grandiflorum* (Liliaceae), and inflorescences of *Ligusticum porteri* (Apiaceae), *Heuchera parviflora* (Saxifragaceae), *Veratrum tenuipetalum, Thalictrum fendleri* (Thalictraceae), and *Lupinus argenteus* (Fabaceae). There can be differences within a genus; for example *Delphinium nuttallianum*, which flowers much earlier than *D. barbeyi*, is not sensitive to frost, and *Erigeron flagellaris*, *E. elatior,* and *E. coulteri* do not seem to suffer frost damage.

In some cases, when most but not all flower buds are killed by frost, it appears that it may be the later-developing buds that survive, as flowering may be delayed beyond what would otherwise be predicted from the time of snowmelt. This could be responsible for the observed correlation between the coefficient of variation of flowering date by *Erigeron* and snowmelt date (Fig. 4). In this species some buds may survive frost, particularly in the rocky meadow plots, which are at a higher altitude and may escape effects of cold air drainage, and the combination of these flowers that may open at a "normal" date and those late-developing buds on plants on which most buds were killed by frost would generate a larger range of flowering dates. Kudo et al. (2008) found that flowering dates of early spring plants were more variable than those of later-flowering species, and attributed this to their dependence on timing of snowmelt.

The effects of frost on wildflowers at this study site are highly variable on a small geographic scale. Cold air drainage appears to play an important role in affecting low-lying areas, and the few degrees difference that this can make over a small scale of altitude was evident in the 2006 frost. In four of the five years in which there was more than a 10% difference between the upper and lower plots in frost kill of flower buds of *Helianthella* plants, the lower plot had the greater level of damage. In 2006, for example, the lower plot had 70% frost kill, and the upper plot 47%. There is 12.3-m difference in altitude between these plots (difference between the mean altitudes of upper and lower edges of each plot), but the minimum June temperatures was −3.37°C in the lower plot and −1.51°C in the upper plot (on 23 June 2006 for both plots; data recorded every 15 minutes with Hobo Pro Series data loggers [Onset, Pocasset, Massachusetts, USA]). The temperature in one of the phenology plots (Wet Meadow 1), which is at 2870 m, was −3.37°C on the same night (but −4.3°C on 16 June), and in this area all of the *Helianthella* flower buds were killed in 2006. In contrast to the high mortality in these plots, there was almost no frost damage in 2006 to

PLATE 1. (Above) *Erigeron speciosus* (Asteraceae) is an important nectar resource for the butterfly *Speyeria mormonia* (Mormon fritillary); (below) a frostkilled bud of *E. speciosus*. Photo credits: D. W. Inouye. A color photograph of *Helianthella quinquenervis* (Asteraceae) is available in the *Bulletin* of the Ecological Society of America 88(4).

Helianthella plants along trail 401, a few hundred meters away from the *Helianthella* plots and about 89 m higher, no frost damage to plants along County Road 317 in Mount Crested Butte (altitude about 2895 m, 5.8 km from RMBL), but 100% mortality at Horse Ranch Park (altitude 2706 m, 18.5 km from RMBL). This variation, even within very similar altitudes, indicates the importance of microclimate in determining both patterns of snowmelt and later air temperature.

Because these plant species are long-lived perennials, it is possible that the loss of reproductive potential due to frost damage to flower buds may not play a significant role in the long-term demography of their populations, if they are not limited by seed input. However, preliminary analysis of data for *Helianthella* from a demographic study at RMBL (D. Inouye, *unpublished data*) shows that the number of plants in a set of six 1.5×5 m plots has decreased significantly over the past nine years. During this period there has been significant recruitment of seedlings in only two years (1998, 2000); no seedlings have been found since 2000, following the last year without significant frost damage

to flower heads (1999, see Fig. 6). If this trend of significant frost damage were to continue for many years, the population decline would probably continue. Even without recruitment, local extinction would take many years given the longevity of the plants.

Although it may seem paradoxical that a consequence of global warming is an increase in the frequency of frost damage, for the species described in this paper, and for those others mentioned that also suffer frost damage, there has been an increase in the past several years in the frequency of frost that damages vegetative or reproductive parts. The observed trend toward lower June minimum temperatures over the past few decades is not predicted by models of global warming, which in fact predict that night-time temperatures may be warming faster than daytime temperatures (Easterling et al. 2000). The phenomenon of earlier snowmelt and greater frost exposure may be a general phenomenon at high altitudes and high latitudes, as it has also been documented in a subarctic tundra community (Wipf et al. 2006). Bannister et al. (2005) suggested that the dependence on day length and temperature for development of frost tolerance of the alpine New Zealand species they examined was likely to confer protection even in the face of global warming, but assumed that incidence of frosts would be reduced. Scheifinger et al. (2003) found that frost events (last occurrence of daily minimum temperatures below a certain threshold) in Europe have been moving faster to earlier occurrence dates than have phenological phases during the preceding decade, and suggested that the risk of late spring frost damage should have been lower as a consequence.

Some animal species may be similarly reliant upon melting of the snowpack to set phenological clocks. For example, laying date and clutch size of American Pipets in alpine Wyoming are correlated with snowmelt date (Hendricks 2003). At my study site, the phenology of bumble bee queen emergence (from spending the winter underground) is probably tied to snowmelt in a fashion similar to that of plant development and flowering (D. Inouye, *personal observation*). Species of seed predators such as the tephritid flies that use *Helianthella* flowers as a host, and overwinter as adults, are probably also linked to snowmelt in their emergence. The abundance of these seed predators seems to have declined significantly in recent years (compared to levels reported in Inouye and Taylor [1979]; D. Inouye, *personal observation*), probably due to loss of opportunities for oviposition in flower heads. It is likely that other species of pollinators and herbivores are also tied phenologically to snowmelt dates.

One recent event that seems to have a significant effect on winter snowfall at my study site, and therefore plays a role in frost damage, is the change of phase of the North Pacific Oscillation (Pacific Decadal Oscillation), which has also been shown to influence precipitation and fire regimes in the Rocky Mountains (Schoennagel et al. 2005). The state of this 50–75 year sea surface temperature cycle has influenced winter precipitation at RMBL (data from 1935 to 2004, $P < 0.05$), and may be responsible in part for the trend toward more precipitation falling as rain instead of snow (Knowles et al. 2006). The phase change in 1998 falls about half-way through the data set for percentage of *Helianthella* flower buds killed by frost. The mean from 1992 to 1998 is 36.1% of buds killed by frost, and for 1999–2006 the mean is 73.9% (t test, $P = 0.06$). This appears to be an example of a regional climate change that is having an effect on phenology and, mediated by the effects of frost, on flowering and potentially plant demography and other species (pollinators, seed predators, parasitoids) involved in the trophic cascade starting with these wildflowers. Climate change at local and global scales may also be having an effect, but is more difficult to discern in this study, although the trend toward lower June minimum temperatures may be an effect at the local scale.

Conclusions

Both the timing and abundance of flowering by the species described in this paper are highly variable, and this variation is strongly influenced by differences among years in the amount of winter snowfall and subsequent snowmelt. Winter precipitation is likely to continue to be relatively light for the next couple of decades, until the next phase change of the North Pacific Oscillation. This supports the conclusion that frost is likely to be an important factor affecting the abundance of flowering in sensitive species, and that a continued reduction in seed production is likely to have demographic consequences.

This and other studies provide strong evidence for ecological constraints on phenological responses to rates of environmental change. Of course not all ecosystems experience frost, and in some cases frost may not be an important factor even if it does occur (e.g., Kudo et al. 2008), but a general message from this study and all the others in this Special Feature is that long-term records may be required to tease out the environmental variables that affect phenology. Non-scientists can contribute to these efforts (Miller-Rushing and Primack 2008), and participation by this audience is a goal of the National Phenology Network. Although I have focused on herbaceous species, it may be important to consider how phenology of woody species may differ (e.g., Rich et al. 2008), and while I focused on a small spatial scale (2×2 m plots), satellite remote sensing can also be a valuable tool for phenological studies (Rich et al. 2008). I focused on flowering phenology, but as Post et al. (2008) point out, not all life history events respond similarly to environmental variation. No matter the scale at which it is measured, or who is collecting the data, it is likely that phenology will become a more common element of scientific studies of the effects of future climate change.

Acknowledgments

Funding and research assistance for this project has been provided by the National Science Foundation (dissertation improvement grant, grants DEB 75-15422, DEB 78-07784, BSR 81-08387, DEB 94-08382, IBN-98-14509, and DEB-0238331), Sigma Xi, an NDEA Title IV predoctoral fellowship, research grants from the University of Maryland's General Research Board, and assistance from Earthwatch and its Research Corps. Research facilities and access to study sites were provided by RMBL, whose NSF grant DBI 0420910 supported collection of high-resolution GPS data; Jessica Boynton assisted with the GPS data collection. John Tuttle has provided access to study sites since 1973. Many research assistants and winter caretakers have helped to collect the phenology data on dates when I was not at RMBL. Graham Pyke collected data from one set of plots in 1973–1974. Snowpack data were provided by billy barr. Doug Gill, Judy Che, Beth Olsen, Abe Miller-Rushing, and two anonymous reviewers provided useful comments on earlier versions of the manuscript, and Brian Inouye provided statistical advice.

Literature Cited

Bannister, P., T. Maegli, K. Dickinson, S. Halloy, A. Knight, J. Lord, A. Mark, and K. Spencer. 2005. Will loss of snow cover during climatic warming expose New Zealand alpine plants to increased frost damage? Oecologia 144:245–256.

Beniston, M., and D. G. Fox. 1996. Impacts of climate change on mountain regions. Pages 191–213 *in* R. T. Watson, M. C. Zinyowera, and R. H. Moss, editors. Climate change 1995: impacts, adaptations and mitigation of climate change. Contribution of Working Group II to the Second Assessment Report of the IPCC. Cambridge University Press, New York, New York, USA.

Cayan, D. R., S. A. Kammerdiener, M. D. Dettinger, J. M. Caprio, and D. H. Peterson. 2001. Changes in the onset of spring in the western United States. Bulletin of the American Meteorological Society 82:399–415.

Dankers, R., and O. B. Christensen. 2005. Climate change impact on snow coverage, evaporation and river discharge in the sub-arctic Tana Basin, Northern Fennoscandia. Climatic Change 69:367–392.

Diaz, H. F., J. K. Eischeid, C. Duncan, and R. S. Bradley. 2003. Variability of freezing levels, melting season indicators, and snow cover for selected high-elevation and continental regions in the last 50 years. Climatic Change 59:33–52.

Easterling, D. R., T. R. Karl, and K. P. Gallo. 2000. Observed climate variability and change of relevance to the biosphere. Journal of Geophysical Research 105:20, 101–120, 114.

Giménez-Benavides, L., A. Escudero, and J. M. Iriondo. 2007. Reproductive limits of a late-flowering high-mountain Mediterranean plant along an elevational climate gradient. New Phytologist 173:367–382.

Grissino-Mayer, H. D., W. H. Romme, M. L. Floyd, and D. D. Hanna. 2004. Climatic and human influences on fire regimes of the southern San Juan mountains, Colorado, USA. Ecology 85:1708–1724.

Hendricks, P. 2003. Spring snow conditions, laying date, and clutch size in an alpine population of American Pipits. Journal of Field Ornithology 74:423–429.

Inouye, D. W. 2000. The ecological and evolutionary significance of frost in the context of climate change. Ecology Letters 3:457–463.

Inouye, D. W., and A. D. McGuire. 1991. Effects of snowpack on timing and abundance of flowering in *Delphinium nelsonii* (Ranunculaceae): implications for climate change. American Journal of Botany 78:997–1001.

Inouye, D. W., M. Morales, and G. Dodge. 2002. Variation in timing and abundance of flowering by *Delphinium barbeyi* Huth (Ranunculaceae): the roles of snowpack, frost, and La Niña, in the context of climate change. Oecologia 139:543–550.

Inouye, D. W., F. Saavedra, and W. Lee. 2003. Environmental influences on the phenology and abundance of flowering by *Androsace septentrionalis* L. (Primulaceae). American Journal of Botany 90:905–910.

Inouye, D. W., and O. R. Taylor. 1979. A temperate region plant-ant-seed predator system: consequences of extrafloral nectar secretion by *Helianthella quinquenervis*. Ecology 60:1–7.

Inouye, D. W., and F. E. Wielgolaski. 2003. High altitude climates. Pages 195–214 *in* M. D. Schwartz, editor. Phenology: an integrative environmental science. Kluwer Academic Publishers, Dordrecht, The Netherlands.

Johnson, T. R. 1998. Climate change and Sierra Nevada snowpack. Thesis. University of California–Santa Barbara, Santa Barbara, California, USA.

Knowles, N., M. D. Dettinger, and D. R. Cayan. 2006. Trends in snowfall versus rainfall in the western United States. Journal of Climate 19:4545–4559.

Kudo, G., and A. Hirao. 2006. Habitat-specific responses in the flowering phenology and seed set of alpine plants to climate variation: implications for global-change impacts. Population Ecology 48:49–58.

Kudo, G., T. Y. Ida, and T. Tani. 2008. Linkages between phenology, pollination, photosynthesis, and reproduction in deciduous forest understory plants. Ecology 89:321–331.

Lynov, Y. S. 1984. Phenological inversions in alpine terrain (Western Tien Shan). Ékologiya 4:29–33.

Miller, P. C. 1982. Environmental and vegetation variation across a snow accumulation area in montane tundra in central Alaska. Holarctic Ecology 5:85–98.

Miller-Rushing, A. J., and R. B. Primack. 2008. Global warming and flowering times in Thoreau's Concord: a community perspective. Ecology 89:332–341.

Post, E. S., C. Pedersen, C. C. Wilmers, and M. C. Forchhammer. 2008. Phenological sequences reveal aggregate life history response to climatic warming. Ecology 89:363–370.

Rich, P. M., D. D. Breshears, and A. B. White. 2008. Phenology of mixed woody–herbaceous ecosystems following extreme events: net and differential responses. Ecology 89: 342–352.

Saavedra, F., D. W. Inouye, M. V. Price, and J. Harte. 2003. Changes in flowering and abundance of *Delphinium nuttallianum* (Ranunculaceae) in response to a subalpine climate warming experiment. Global Change Biology 9:885–894.

Scheifinger, H., A. Menzel, E. Koch, and C. Peter. 2003. Trends of spring time frost events and phenological dates in Central Europe. Theoretical and Applied Climatology 74:41–51.

Schoennagel, T., T. T. Veblen, W. H. Romme, J. S. Sibold, and E. R. Cook. 2005. ENSO and PDO variability affect drought-induced fire occurrence in Rocky Mountain subalpine forests. Ecological Applications 15:2000–2014.

Visser, M. E., A. J. Van Noordwijk, J. M. Tinbergen, and C. M. Lessells. 1998. Warmer springs lead to mistimed reproduction in Great Tits (*Parus major*). Proceedings of the Royal Society London, Series B 265:1867–1870.

Wielgolaski, F. E., and D. W. Inouye. 2003. High latitude climates. Pages 175–194 *in* M. D. Schwartz, editor. Phenology: an integrative environmental science. Kluwer Academic Publishers, Dordrecht, The Netherlands.

Wipf, S., C. Rixen, and C. P. H. Mulder. 2006. Advanced snowmelt causes shift towards positive neighbour interactions in a subarctic tundra community. Global Change Biology 12:1496–1506.

LETTERS

Southern Ocean deep-water carbon export enhanced by natural iron fertilization

Raymond T. Pollard[1], Ian Salter[1,2], Richard J. Sanders[1], Mike I. Lucas[3], C. Mark Moore[1], Rachel A. Mills[1], Peter J. Statham[1], John T. Allen[1], Alex R. Baker[4], Dorothee C. E. Bakker[4], Matthew A. Charette[5], Sophie Fielding[6], Gary R. Fones[7], Megan French[4], Anna E. Hickman[8], Ross J. Holland[1], J. Alan Hughes[1], Timothy D. Jickells[4], Richard S. Lampitt[1], Paul J. Morris[1], Florence H. Nédélec[9], Maria Nielsdóttir[1], Hélène Planquette[10], Ekaterina E. Popova[1], Alex J. Poulton[1], Jane F. Read[1], Sophie Seeyave[1], Tania Smith[1], Mark Stinchcombe[1], Sarah Taylor[1], Sandy Thomalla[11], Hugh J. Venables[6], Robert Williamson[11] & Mike V. Zubkov[1]

The addition of iron to high-nutrient, low-chlorophyll regions induces phytoplankton blooms that take up carbon[1–3]. Carbon export from the surface layer and, in particular, the ability of the ocean and sediments to sequester carbon for many years remains, however, poorly quantified[3]. Here we report data from the CROZEX experiment[4] in the Southern Ocean, which was conducted to test the hypothesis that the observed north–south gradient in phytoplankton concentrations in the vicinity of the Crozet Islands is induced by natural iron fertilization that results in enhanced organic carbon flux to the deep ocean. We report annual particulate carbon fluxes out of the surface layer, at three kilometres below the ocean surface and to the ocean floor. We find that carbon fluxes from a highly productive, naturally iron-fertilized region of the sub-Antarctic Southern Ocean are two to three times larger than the carbon fluxes from an adjacent high-nutrient, low-chlorophyll area not fertilized by iron. Our findings support the hypothesis that increased iron supply to the glacial sub-Antarctic may have directly enhanced carbon export to the deep ocean[5]. The CROZEX sequestration efficiency[6] (the amount of carbon sequestered below the depth of winter mixing for a given iron supply) of 8,600 mol mol^{-1} was 18 times greater than that of a phytoplankton bloom induced artificially by adding iron[7], but 77 times smaller than that of another bloom[8] initiated, like CROZEX, by a natural supply of iron. Large losses of purposefully added iron can explain the lower efficiency of the induced bloom[6]. The discrepancy between the blooms naturally supplied with iron may result in part from an underestimate of horizontal iron supply.

In many open ocean regions there is low phytoplankton biomass despite there being a large macronutrient reservoir[3]. The Southern Ocean is the most biogeochemically significant of these high-nutrient, low-chlorophyll (HNLC) regions, owing to its large spatial extent and influence on global nutrient cycles[9]. Mesoscale iron enrichment experiments have demonstrated that iron addition modifies phytoplankton processes, enhancing diatom biomass[10,11] and increasing atmospheric carbon dioxide drawdown[1]. Observing bloom decline and quantifying the sequestration of photosynthetically fixed carbon resulting from iron addition has been achieved more rarely[7,12].

An alternative way to determine the role of iron in regulating the biological carbon pump in the Southern Ocean is to study regions of high phytoplankton biomass stimulated by natural iron inputs from shallow topography or islands. Recently KEOPS[8] (the Kerguelen ocean and plateau compared study) demonstrated enhanced carbon export to below 200 m in the naturally iron-fertilized bloom over the Kerguelen plateau. The Crozet Islands and Plateau (hereafter Crozet), located in the Polar Frontal Zone at the northern boundary of the Southern Ocean, is another region characterized by a marked annual phytoplankton bloom (Fig. 1). The sub-Antarctic Front of the generally eastward-flowing Antarctic Circumpolar Current turns north past Crozet (Fig. 1) and then east again when it encounters the Agulhas Return Current[13]. Thus, south of Crozet HNLC conditions prevail[4], whereas north of Crozet an annual bloom covering 120,000 km^2 (the size of Ireland and 50 times larger than the SOFeX (Southern Ocean iron experiment) bloom[2,11]) results from iron supplied from Crozet[14]. Iron enrichment over the light-limited winter period leads in spring to a strong north–south gradient in phytoplankton biomass (Fig. 1), productivity, community structure[15] and uptake of dissolved inorganic carbon[16] and nitrate[17], once stratification and increased solar irradiance reduce the mixed layer below the critical depth[18]. Weak circulation in the bloom region is such that water has a residence time there of ~60 days[4].

During austral summer 2004–2005, we conducted an extensive oceanographic research programme (CROZEX) around Crozet[4] to test the hypotheses that the north–south gradient in chlorophyll *a* is, first, induced by natural iron fertilization and, second, causes enhanced organic carbon flux into the deep ocean. To capture this flux, sediment traps were moored north (M10), east (M5) and south (M2, M6) of Crozet (Fig. 1). Short sediment cores were collected at M5, M6 and M10. Weak eastward flow past M2 and M6 and the absence of upstream blooms[13] characterized these HNLC 'control' (−Fe) sites south of the bloom. M10 was under the bloom (+Fe) and M5 was under the eastward extension of the bloom. East–southeast flow along the sub-Antarctic Front towards M5, the large spatial extent of the bloom combined with weak circulation within it and the predominance of *Eucampia antarctica* (a diatom that responded strongly to iron enrichment[19]) in the 3,000-m M10 and M5 traps (but

[1]National Oceanography Centre Southampton, Natural Environment Research Council and University of Southampton, European Way, Southampton SO14 3ZH, UK. [2]Observatoire Océanologique, Avenue de Fontaulé, BP44, F-66651 Banyuls-sur-Mer, France. [3]Department of Zoology, University of Cape Town, Rondebosch 7701, South Africa. [4]School of Environmental Sciences, University of East Anglia, Norwich NR4 7TJ, UK. [5]Department of Marine Chemistry and Geochemistry MS25, Woods Hole Oceanographic Institution, Woods Hole, Massachusetts 02543, USA. [6]British Antarctic Survey, High Cross, Madingley Road, Cambridge CB3 0ET, UK. [7]School of Earth and Environmental Sciences, University of Portsmouth, Burnaby Building, Burnaby Road, Portsmouth PO1 3QL, UK. [8]Department of Earth and Ocean Sciences, University of Liverpool, L69 3GP, UK. [9]Laboratoire Environnement et Resources de Normandie, IFREMER, Avenue du Général de Gaulle - B.P.32, 14 520 Port-en-Bessin, France. [10]Institute of Marine and Coastal Sciences, Rutgers University, New Brunswick, New Jersey 08901, USA. [11]Department of Oceanography, University of Cape Town, Rondebosch 7701, South Africa.

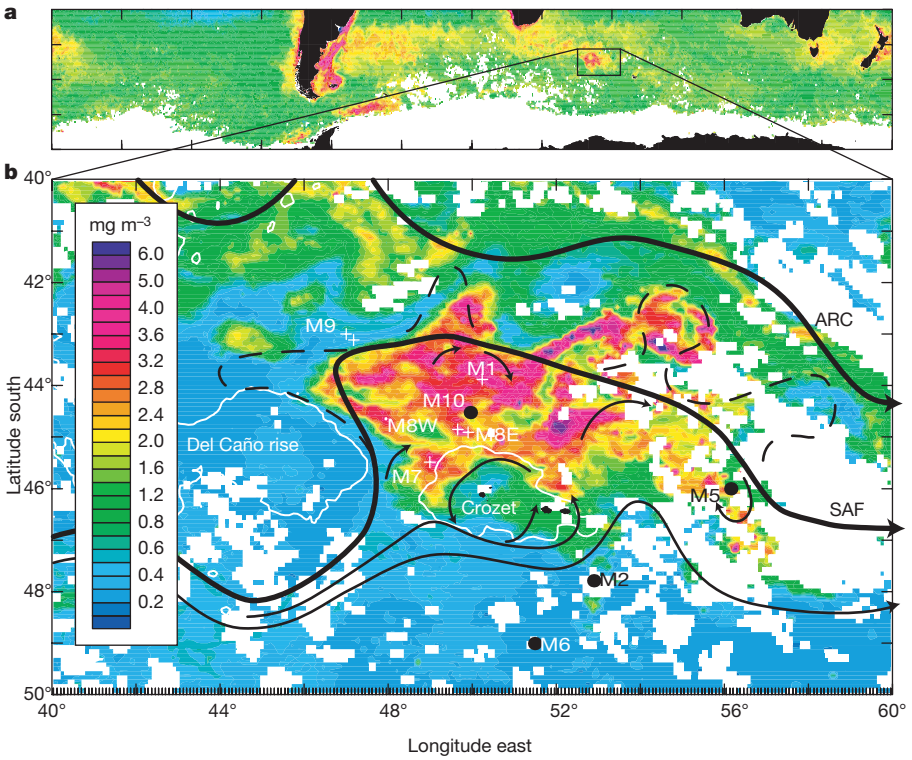

Figure 1 | Chlorophyll *a* images of Crozet region. **a**, Chlorophyll *a* in October for the whole of the Southern Ocean, showing location of Crozet. Colour indicates concentration as shown in **b**. **b**, Merged SeaWiFS/MODIS (sea-viewing, wide-field-of-view sensor/moderate-resolution imaging spectroradiometer) chlorophyll *a* image for the eight-day peak bloom period 23–30 October 2004. Solid and dashed lines show mean and eddy circulations, respectively[13], with the sub-Antarctic Front (SAF, the northern boundary of the Antarctic Circumpolar Current) and the Agulhas Return Current (ARC) shown bold. Main sampling (+) and coring (•) sites are labelled. Thin white lines are the 2,000-m depth contour, with the main Crozet Islands (Île de la Possession, Île de l'Est) seen at 46.5° S, 52° E.

its absence from the M2 and M6 traps) confirm that the M10 and M5 traps received export flux from the iron-enhanced bloom. KEOPS and CROZEX are compared in Supplementary Table 1.

It has been shown[14] that the dissolved iron (DFe; <0.2-μm fraction) originates from Crozet, with maximum estimated input to the bloom of 550 nmol m^{-2} d^{-1} comprising 390, 60 and 100 nmol m^{-2} d^{-1} for the horizontal, vertical and atmospheric fluxes, respectively. As the bloom occurs in deep (>2,000-m) water away from Crozet, horizontal flux dominates DFe supply, as expected. A range of 180–390 nmol m^{-2} d^{-1} (0.018–0.039 mmol m^{-2} integrated over a winter period of 100 days) is estimated (Supplementary Information) for the enhancement in iron supply to the +Fe region relative to that to the −Fe region. These are probably underestimates, as additional sources of iron such as the dissolution of small lithogenic particles[20] will increase iron supply.

Significant differences were observed in the magnitude, timing, duration and community structure of plankton blooms between the +Fe and −Fe regions. In the −Fe region, chlorophyll *a* peaked at 0.6 mg m^{-3} in early December (Fig. 2a), when HNLC conditions (nitrate concentration, ~24 μmol kg^{-1}; silicate concentration, ~16 μmol kg^{-1}) prevailed[4]. In the +Fe region, chlorophyll *a* peaked at over 3 mg m^{-3} in October (locally >6 mg m^{-3}; Fig. 1) and was elevated (>1 mg m^{-3}) for 72 days[18] (Supplementary Table 2). Although fertilized by macronutrients from the −Fe region and by winter upwelling in the Polar Frontal Zone, silicate was already becoming limited (<2 μmol kg^{-1}; nitrate, 16 μmol kg^{-1}) when first sampled in November[4], indicating a ratio of silicate drawdown to nitrate drawdown of about 2:1, consistent with lower iron stress than in the −Fe region[19]. Low ambient silicate concentrations, common over much of the sub-Antarctic Southern Ocean[11], predisposed a shift in phytoplankton community structure from diatoms to *Phaeocystis*[15]. The bloom peaked <10 days after exceeding

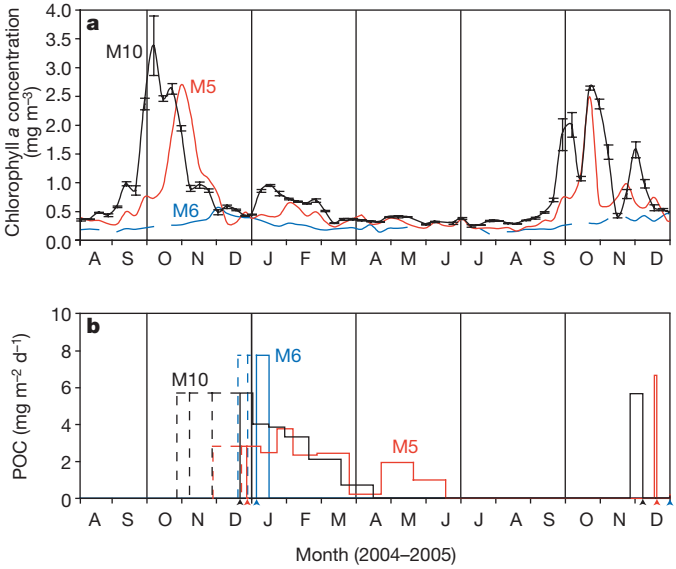

Figure 2 | Time series of chlorophyll *a* and particulate organic carbon (POC). **a**, Chlorophyll *a*, obtained for each eight-day merged SeaWiFS/MODIS image by averaging all non-cloud pixels in a circle of radius 45 km about each mooring site. Error bars (for M10 only) give the standard deviation of the mean of these pixels. **b**, POC (solid line) obtained from deep sediment traps at each site (Methods). Arrowheads mark mooring deployment and recovery events. The traps could not be deployed until after export from the 2004–2005 bloom had begun, so the export rate into the first cup has been extrapolated (Supplementary Information) using a range of sinking rates after the peak of chlorophyll *a* to give minimum, mean and maximum (dashed) seasonal integrals of total export.

1 mg m^{-3} but remained >1 mg m^{-3} for another month, potentially sustained by *Phaeocystis* using regenerated iron and nitrogen[21], as +Fe nitrate values remained ~16 μmol kg^{-1} throughout December and January.

An important difference from purposeful iron enrichment experiments is that iron concentrations accumulate in the +Fe region during winter. Removal of light limitation in spring[18], not iron addition, determines bloom onset. Consequently, net growth rates in the bloom phase (0.05 d^{-1}; Fig. 2a) are probably light limited and 2–18 times lower than those for artificial experiments (0.10–0.90 d^{-1})[3]. Weak circulation in the +Fe region ensures that neither macronutrients nor iron can be resupplied to the extensive bloom area during the bloom development period. A possible exception was close to the islands, where a small-area bloom in January[18] may have been fuelled by resupply of iron and silicate.

The flux of organic carbon from the surface ocean to the ocean interior has been calculated using ^{234}Th at 100 m (ref. 22; Table 1). Following the chlorophyll peak (Fig. 2a) in each region (+Fe, −Fe), mean daily rates of carbon export were similar (16 mmol m^2 d^{-1}; Supplementary Table 2). Thus, any difference in seasonally integrated export between the two regions depends on the duration of the export events. We estimated export duration by closing the silicate budget, dividing the near-surface silicate drawdown (corrected for biogenic silica production) by the opal export rate estimated from ^{234}Th deficits and ^{234}Th/opal ratios. This approach yielded export durations (61 and 17 days in the +Fe and −Fe regions, respectively) consistent with the observed satellite-derived chlorophyll time series (Fig. 2, Supplementary Table 2). The resulting seasonally integrated carbon export in the +Fe region (960 mmol m^{-2}) was three times greater (Table 1) than export in the −Fe region (290 mmol m^{-2}), consistent with the independently diagnosed increase in new production[17].

Fluxes of particulate organic carbon (POC) to 3,000 m differed remarkably in duration and composition. In the +Fe region (Fig. 2b), POC flux peaked at or before trap deployment in late December, decreasing to near zero over several months. In the −Fe region, POC export was confined to an unusually short but substantial event (Fig. 2b) observed at both M2 and M6 and at two depths (for sinking rates and export flux ranges, see Supplementary Information). Substantial silicate drawdown between November and January (Supplementary Table 2) reduced surface silicate to <2.0 μmol kg^{-1} at M2 and M6, suggesting that iron limitation in the −Fe region resulted in heavily silicified diatoms[23] that sank rapidly in January. Despite this event, the longer duration of POC flux over the 2004–2005 summer season in the +Fe region resulted in three times greater seasonal export in the +Fe region than the −Fe region (Table 1). POC flux at 3,000 m was 3% of that at 100 m in the +Fe region and 4% of that at 100 m in the −Fe region (Table 1), indicating that remineralization rates were marginally enhanced by iron availability.

Table 1 | Seasonally integrated carbon fluxes at naturally iron fertilized and HNLC sites and the sequestration efficiency, C/Fe

	Carbon (mmol m^{-2} y^{-1})		C/Fe‖ (mol mol^{-1})
	+Fe (fertilized)	−Fe (HNLC)	
^{234}Th via Si* at 100 m	960	290	17,190
Range	626–1,252	166–415	5,420–60,360
Deep flux† at 3,000 m	25.0	7.1	—
Best estimate‡	28.9	11.6	440
Range‡	25.0–34.2	7.1–17.4	195–1,506
Core top§	9.3 ± 0.5	4.5 ± 0.4	123
Interpolated flux at 150 m¶	642	194	11,487
Interpolated flux at 200 m¶	483	146	8,641

* Summarized from Supplementary Table 2.
† From Fig. 2.
‡ Summarized from Supplementary Information.
§ Summarized from Supplementary Table 3.
‖ Calculated from the differences between +Fe and −Fe carbon fluxes divided by winter-period iron supply (0.018–0.039 mmol m^{-2}).
¶ Calculated from 100-m flux (F) values using a Martin curve $F(z) = F(100\,\text{m}) \times (z/100)^b$, where $b = -0.99$ to fit the 3,000-m carbon flux values.

The organic carbon content of the core-top (surface-mixed-layer) sediments sampled several times during separate corer deployments was significantly higher in the +Fe region than the –Fe region (Supplementary Table 3). Significant sediment focusing and winnowing occurs in this region and thus data are expressed as ^{230}Th$_{xs}$-corrected, preserved fluxes (equivalent to the preserved vertical rain rate at the sea floor). A twofold increase in the ^{230}Th$_{xs}$-corrected, preserved, core-top, organic carbon accumulation was observed in the +Fe region relative to the –Fe region (Table 1). This is consistent with published data from a suite of export production proxies that imply enhanced phytoplankton growth, export and burial throughout the Holocene epoch at this site[24].

Our analyses thus indicate that shallow, seasonally integrated export, annually integrated deep-water POC flux and core-top organic carbon accumulation were all enhanced two- to threefold as a result of the iron-fertilized bloom (Table 1). Our results support Martin's hypothesis[5] that relief of iron deficiency enhances carbon sequestration into the deep ocean (here >3,000 m) and sediment. Results from CROZEX thus support increased atmospheric iron deposition[1] as a mechanism for the inferred increase in organic carbon flux in the sub-Antarctic during the Last Glacial Maximum[24,25].

The ratio of carbon exported below some depth to iron added at the surface, (C/Fe) is termed the export efficiency or (if below the depth of winter mixing) sequestration efficiency[6,8]. Our ^{234}Th-derived estimates of the seasonal enhanced (+Fe minus −Fe) POC flux at 100 m (670 mmol m^{-2}) and additional iron supply (0.039 mmol m^{-2}) lead to a C/Fe ratio (at 100 m) of 17,200 mol mol^{-1} (range, 5,400–60,400; Table 1). This value for the shallow export efficiency from CROZEX was somewhat higher than comparable values from iron-addition experiments (6,600 for SOFeX[12], 1,200 for SERIES (the sub-Arctic ecosystem response to iron enrichment study)[7]). Interpolating with a Martin curve[26] to a winter mixed-layer depth of 150–200 m (ref. 18), we further calculated a seasonal C/Fe sequestration efficiency of 11,500–8,600 (Table 1), compared with previous estimates of 500–3,300 (refs 7, 12) and the KEOPS[8] seasonal estimate of 668,000. Given the different methods used to estimate both additional iron supply and carbon export between studies[3,7,8,12], the reasons for the wide range of export efficiencies are unclear. However, we note that the KEOPS result depends on a combination of an eightfold-lower estimate for seasonal iron supply and a tenfold-higher estimate for carbon export (Supplementary Table 1). It is possible that iron supply was higher to the KEOPS bloom before the late-summer observation period on which the seasonal iron supply was based, owing either to enhanced vertical supply before surface-water stratification in spring, coupled with luxury iron uptake[27] (that is, more than is absolutely necessary), or to horizontal input of lithogenic material from nearby islands[28,29].

The results from CROZEX indicate that natural iron fertilization enhanced new production[17] and near-surface export at 100 m two- to threefold (Table 1). Moreover, we present evidence that carbon fluxes at 3,000 m and the sediment were similarly two to three times higher beneath the natural fertilized region than for a nearby HNLC region with similar end-of-winter macronutrient concentrations. Carbon sequestered past 200 m was only 50% of that exported past 100 m. Although the CROZEX estimate of carbon sequestration for a given iron supply was 20 times that of SERIES[7], it still falls 15–50 times short of some geo-engineering estimates[6], with significant implications for proposals to mitigate the effects of climate change through purposeful addition of iron to the ocean.

METHODS SUMMARY

Chlorophyll was determined using remote-sensing techniques referenced to *in situ* data. Iron concentrations in the bloom were estimated using a simple model including horizontal and vertical advection and atmospheric deposition. Organic carbon and opal export rates were determined using ^{234}Th deficits

and ^{234}Th/opal and organic carbon ratios from large particles. Biogenic silica was determined by spectrophotometric analysis of silicate levels in digested filtered samples. Sediment traps were McClane traps. Core data were derived from analysis of multiple gravity and Megacorer-derived samples.

Full Methods and any associated references are available in the online version of the paper at www.nature.com/nature.

Received 23 October; accepted 8 December 2008.

1. Watson, A. J., Bakker, D. C. E., Ridgwell, A. J., Boyd, P. W. & Law, C. S. Effect of iron supply on Southern Ocean CO_2 uptake and implications for glacial atmospheric CO_2. *Nature* **407,** 730–733 (2000).
2. De Baar, H. J. W. *et al.* Synthesis of iron fertilization experiments: From the iron age in the age of enlightenment. *J. Geophys. Res.* **110,** doi:10.1029/2004JC002601 (2005).
3. Boyd, P. W. *et al.* Mesoscale iron enrichment experiments 1993–2005: Synthesis and future directions. *Science* **315,** 612–617 (2007).
4. Pollard, R. T., Sanders, R., Lucas, M. I. & Statham, P. J. The Crozet Natural Iron Bloom and Export Experiment (CROZEX). *Deep-Sea Res. II* **54,** 1905–1914 (2007).
5. Martin, J. H. Glacial-interglacial CO_2 change: the iron hypothesis. *Paleoceanography* **5,** 1–13 (1990).
6. Buesseler, K. O. & Boyd, P. W. Will ocean fertilization work? *Science* **300,** 67–68 (2003).
7. Boyd, P. W. *et al.* The decline and fate of an iron-induced subarctic phytoplankton bloom. *Nature* **428,** 549–553 (2004).
8. Blain, S. *et al.* Effect of natural iron fertilization on carbon sequestration in the Southern Ocean. *Nature* **446,** 1070–1074 (2007).
9. Sarmiento, J. L., Gruber, N., Brzezinski, M. A. & Dunne, J. P. High-latitude controls of thermocline nutrients and low latitude biological productivity. *Nature* **427,** 56–60 (2004).
10. Boyd, P. W. *et al.* A mesoscale phytoplankton bloom in the polar Southern Ocean stimulated by iron fertilization. *Nature* **407,** 695–702 (2000).
11. Coale, K. *et al.* Southern Ocean iron enrichment experiment: Carbon cycling in high- and low-Si waters. *Science* **304,** 408–414 (2004).
12. Buesseler, K. O., Andrews, J. E., Pike, S. M. & Charette, M. A. The effects of iron fertilization on carbon sequestration in the Southern Ocean. *Science* **304,** 414–417 (2004).
13. Pollard, R. T., Venables, H. J., Read, J. F. & Allen, J. T. Large scale circulation around the Crozet Plateau controls an annual phytoplankton bloom in the Crozet Basin. *Deep-Sea Res. II* **54,** 1915–1929 (2007).
14. Planquette, H. F. *et al.* Dissolved iron in the vicinity of the Crozet Islands, Southern Ocean. *Deep-Sea Res. II* **54,** 1999–2019 (2007).
15. Poulton, A. J. *et al.* Phytoplankton community composition around the Crozet Plateau, with emphasis on diatoms and *Phaeocystis*. *Deep-Sea Res. II* **54,** 2085–2105 (2007).
16. Bakker, D. C. E., Nielsdóttir, M. C., Morris, P. J., Venables, H. J. & Watson, A. J. The island mass effect and biological carbon uptake for the subantarctic Crozet Archipelago. *Deep-Sea Res. II* **54,** 2174–2190 (2007).
17. Sanders, R. *et al.* New production and the f-ratio around the Crozet Plateau in austral summer 2004–2005 diagnosed from seasonal changes in inorganic nutrient levels. *Deep-Sea Res. II* **54,** 2191–2207 (2007).
18. Venables, H. J., Pollard, R. T. & Popova, E. K. Physical conditions controlling the development of a regular phytoplankton bloom north of the Crozet Plateau, Southern Ocean. *Deep-Sea Res. II* **54,** 1949–1965 (2007).
19. Moore, C. M., Hickman, A. E., Poulton, A. J., Seeyave, S. & Lucas, M. I. Iron-light interactions during the CROZet natural iron bloom and EXport experiment (CROZEX) II: taxonomic responses and elemental stoichiometry. *Deep-Sea Res. II* **54,** 2066–2084 (2007).
20. Planquette, H. F. *Iron Biogeochemistry in the Waters Surrounding the Crozet Islands, Southern Ocean.* PhD thesis, Southampton Univ. (2008).
21. Lucas, M. I., Seeyave, S., Sanders, R., Moore, C. M. & Williamson, R. Nitrogen uptake responses to a naturally Fe-fertilised phytoplankton bloom during the 2004/2005 CROZEX study. *Deep-Sea Res. II* **54,** 2138–2173 (2007).
22. Morris, P. J., Sanders, R., Turnewitsch, R. & Thomalla, S. ^{234}Th-derived particulate organic carbon export compared to new production from an island induced phytoplankton bloom in the Southern Ocean. *Deep-Sea Res. II* **54,** 2208–2232 (2007).
23. Franck, V. M., Brzezinski, M. A., Coale, K. H. & Nelson, D. M. Iron and silicic acid concentrations regulate Si uptake north and south of the Polar Frontal Zone in the Pacific Sector of the Southern Ocean. *Deep-Sea Res. II* **47,** 3315–3338 (2000).
24. Marsh, R., Mills, R. A., Green, D. R. H., Salter, I. & Taylor, S. Controls on sediment geochemistry in the Crozet region. *Deep-Sea Res. II* **54,** 2260–2274 (2007).
25. Kohfeld, K. E., Le Quéré, C., Harrison, S. P. & Anderson, R. F. Role of marine biology in glacial-interglacial CO_2 cycles. *Science* **308,** 74–78 (2005).
26. Buesseler, K. O. *et al.* Revisiting carbon flux through the ocean's twilight zone. *Science* **316,** 567–570 (2007).
27. Mongin, M., Molina, E. & Trull, T. W. Seasonality and scale of the Kerguelen plateau phytoplankton bloom: a remote sensing and modeling analysis of the influence of natural iron fertilization in the Southern Ocean. *Deep-Sea Res. II* **55,** 880–892 (2008).
28. Zhang, Y., Lacan, F. & Jeandel, C. Dissolved rare earth elements tracing lithogenic inputs over the Kerguelen Plateau (Southern Ocean). *Deep-Sea Res. II* **55,** 638–652 (2008).
29. van Beek, P. *et al.* Radium isotopes to investigate the water mass pathways on the Kerguelen Plateau (Southern Ocean). *Deep-Sea Res. II* **55,** 622–637 (2008).

Supplementary Information is linked to the online version of the paper at www.nature.com/nature.

Acknowledgements We thank the operators, master and crew of RRS *Discovery* for their support. CROZEX was a component of Biophysical Interactions and Controls on Export Production, a five-year project at the National Oceanography Centre, Southampton, supported by the Natural Environment Research Council (NERC).

Author Contributions R.T.P. led the project, the first cruise and the physics analysis (J.T.A., J.F.R., H.J.V). R.J.S. led the second cruise and the nutrient chemistry analysis (M.F., R.S.L., P.J.M., I.S., M.S., S.T.), P.J.S. the iron and radium chemistry analysis (A.R.B., M.A.C., G.R.F., T.D.J., F.H.N., H.P.), M.I.L. the biology analysis (C.M.M., S.F., A.E.H., R.J.H., A.J.P., S.S., R.W., M.V.Z.), D.C.E.B. the carbon dioxide chemistry analysis (M.N.), R.A.M. the sediment chemistry analysis (S.T.) and J.A.H. the benthic biology analysis (T.S.). R.T.P. wrote the paper, assisted by R.J.S., C.M.M., I.S. (sediment traps), H.F.P. (iron), P.J.M (^{234}Th), R.A.M. (cores) and M.I.L. (biology), with all authors commenting.

Author Information Data are held at the British Oceanographic Data Centre (http://www.bodc.ac.uk). Reprints and permissions information is available at www.nature.com/reprints. Correspondence and requests for materials should be addressed to R.J.S. (rics@noc.soton.ac.uk).

METHODS

Chlorophyll *a*. Chlorophyll *a* (Figs 1 and 2) was determined from NASA's merged SeaWiFS/MODIS products, adjusted to match *in situ* data[18].

Iron concentrations in the bloom region[14]. Iron concentrations were estimated by considering lateral advection of DFe from the islands into the surrounding water, vertical mixing of iron from beneath the seasonal thermocline and atmospheric deposition. Total dissolved iron concentrations (DFe $<$0.2-μm fraction) were determined using flow-injection catalytic spectrophotometric detection. Horizontal iron flux was estimated from samples of DFe collected along a series of stations extending seawards from the northern coast of Île de la Possession and by using the terrestrially derived, short-lived radium isotopes ^{223}Ra and ^{224}Ra to estimate horizontal mixing coefficients at the same stations[30]. Horizontal gradients in these species were combined with estimates of the plateau circumference to estimate total DFe release from the plateau over the 100-day winter period when the mixed-layer depth is such that the surface ocean is in contact with plateau sediments. Vertical iron flux was diagnosed from analysis of ^{228}Ra and DFe profiles. Finally, the estimated atmospheric (wet and dry) iron flux was based on calcium and silicon concentrations in aerosols and DFe measurements in rain samples by ICP-OES (inductively coupled plasma-optical emission spectrometer). The flux of DFe to surface waters was extrapolated to, and integrated over, the winter period. Values are consistent with atmospheric dust transport models.

Organic carbon and opal export. Shallow rates were estimated by multiplying the observed 0–100-m deficit of the short-lived natural radioisotope ^{234}Th by the ^{234}Th/POC or ^{234}Th/Opal ratio in large-volume samples of large particulate material ($>$53 μm) collected using a Stand-Alone Pumping System deployed approximately 20 m below the mixed layer[22].

Biogenic silica. Measurements of biogenic silica were made on 1-litre seawater samples filtered onto 0.4-μm polycarbonate filters, stored at $-20\,^{\circ}$C, digested in 0.2 mol sodium hydroxide and neutralized with 0.1 mol hydrochloric acid[31,32] and analysed using a Skalar Sanplus autoanalyser. Opal accumulation was estimated by integrating values in the upper 100 m.

Sediment traps. Traps were McLane 21-cup time-series arrays deployed on bottom-tethered moorings. Sampling bottles were filled with buffered preservative solution according to Joint Global Ocean Flux Study protocols. Upon recovery, samples were filtered through a 1-mm Nitex mesh. Swimmers were carefully removed from the $<$1-mm fraction. The $>$1-mm fraction was comprised exclusively of large swimmers. Some cups were contaminated by fish (*Notolepis coatsi*) feeding on the sinking material. All fish debris was picked out by hand. All chemical analysis was performed on the $<$1-mm fraction after it had been freeze-dried and homogenized. Following acidification with hydrochloric acid, particulate organic carbon and nitrogen were measured using a Carlo Erba NA 1500 elemental analyser following standardization with acetanilide.

Core-top accumulation rates. A Megacorer was used to obtain sediment cores with an undisturbed sediment–water interface and gravity core deployments were used to sample deeper sediments. Samples from the surface mixed layer (0–10 cm below the surface) were dried, ground and subjected to the same methodology as described for the sediment trap material for particulate organic carbon and nitrogen at the National Oceanography Centre, Southampton, and NERC Isotope Geosciences Laboratory. U-series isotopes were determined by isotope dilution multi-collector ICP-MS (inductively coupled plasma mass spectrometry) at the Department of Earth Sciences, University of Oxford. ^{230}Th-normalized, preserved organic carbon fluxes were estimated from the sediment composition and the ^{230}Th-normalized sediment accumulation rate (measured ^{238}U/^{232}Th activity ratio of detrital end-member is 0.9). These data supplement published data[24] also tabulated for comparison.

30. Charette, M. *et al.* Radium isotopes as tracers of iron sources fueling a Southern Ocean phytoplankton bloom. *Deep-Sea Res. II* **54,** 1989–1998 (2007).
31. Brown, L., Sanders, R., Savidge, G. & Lucas, C. H. The uptake of silica during the spring bloom in the Northeast Atlantic Ocean. *Limnol. Oceanogr.* **48,** 1831–1845 (2003).
32. Poulton, A. J. *et al.* Phytoplankton mineralisation in the tropical and subtropical Atlantic Ocean. *Glob. Biogeochem. Cycles* **20,** BG4002 (2006).

Ocean Storage of CO_2

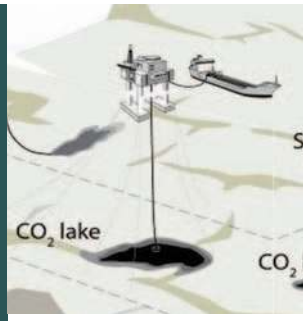

E. Eric Adams[1] and Ken Caldeira[2]

1811-5209/08/0004-0319$2.50 DOI: 10.2113/gselements.4.5.319

One method for minimizing climate change is to capture CO_2 from power plants and inject it into the deep ocean, thus reducing the magnitude and rate of change of CO_2 concentration in the atmosphere and the surface ocean. Many discharge options are possible, with varied mixing and retention characteristics. The ocean's capacity is vast, and mathematical models suggest that injected CO_2 could remain sequestered for several hundred years. While theoretical and laboratory studies support the viability of ocean storage, field experiments are necessary to realistically evaluate the environmental impact.

KEYWORDS: ocean carbon sequestration, CO_2 ocean storage, environmental impact, climate change

INTRODUCTION

Other articles in this issue discuss the motivation for carbon dioxide (CO_2) capture and storage as a method to help combat global climate change (Oelkers and Cole 2008; Broecker 2008). In particular, storage in underground reservoirs is highlighted (Benson and Cole 2008; Oelkers et al. 2008). Here we describe the possibilities for CO_2 storage in the deep ocean, focusing on direct-injection strategies that could be applied on an industrial scale.

There are several reasons for considering the deep ocean as a sink for anthropogenic CO_2. First, the ocean has a vast uptake capacity. It currently contains an estimated 40,000 Gt C (billion tons of carbon), mostly in the form of dissolved inorganic ions. This compares with about 800 Gt C contained in the atmosphere and 2000 Gt C in the land biosphere. Thus, the amount of carbon that would cause a doubling of the atmospheric concentration would only change the ocean concentration by about 2%. Second, we are already discharging CO_2 indirectly into the surface ocean when we emit it to the atmosphere. Because emissions are large, the atmosphere and ocean are currently out of chemical equilibrium, causing a net flux of about 8 Gt CO_2 per year (2 Gt C per year) to the ocean. Over a period of centuries, 70–80% of present-day emissions will ultimately reside in the ocean. Discharging CO_2 directly into the deep ocean would accelerate this natural process, thus reducing peak atmospheric concentrations and protecting ocean surface waters with a slower rate of CO_2 increase. FIGURE 1 presents the results of simulations for the reduction in atmospheric CO_2 concentration that could be achieved using several release–uptake scenarios in which known fossil fuel reserves are consumed (Kheshgi and Archer 2004). Compared with releasing all CO_2 to the atmosphere, as happens now, introducing half to the deep ocean would reduce the peak concentration by a factor of about two. However, the ocean and atmosphere systems are closely coupled, so even if all anthropogenic CO_2 were injected directly into the oceans, some would return to the atmosphere through degassing.

Over the past 200 years, oceans have taken up over 500 Gt of CO_2 from the atmosphere, compared with over 1300 Gt CO_2 emitted to the atmosphere (IPCC 2005). As a result, the pH of the surface ocean (the upper few hundred meters that are in greatest contact with the atmosphere) has dropped by about 0.1 pH units from the preindustrial value of about 8.2. This causes concern for the health of coral reefs and other organisms that use calcium carbonate in their skeletons or shells. FIGURE 2 presents model results for ocean pH if known fossil fuel reserves are burned and CO_2 is released. The atmospheric concentration would increase to ~2000 ppm in 300 years (similar to FIGURE 1), and ocean

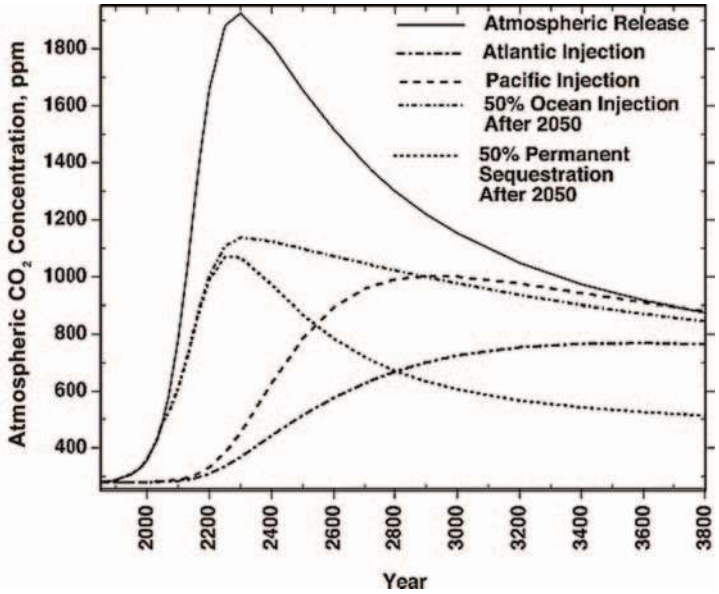

FIGURE 1 Simulated atmospheric CO_2 concentration (ppm) resulting from release of 18,000 Gt CO_2 to the atmosphere, to the ocean at 3000 m below sea level, or to a combination of both. ADAPTED FROM KHESHGI AND ARCHER (2004), WITH PERMISSION FROM THE AMERICAN GEOPHYSICAL UNION

1 Department of Civil and Environmental Engineering
Massachusetts Institute of Technology, Room 48-216b
Cambridge, MA 02139, USA
E-mail: eeadams@mit.edu

2 Department of Global Ecology, Carnegie Institution
Stanford University, 260 Panama St., Stanford, CA 94305, USA
E-mail: kcaldeira@stanford.edu

surface pH would drop by more than 0.7 units (Caldeira and Wickett 2003). By injecting some of the CO_2 into the deep ocean, the time until it disperses to surface water is extended, allowing the change in pH to be distributed more uniformly with depth.

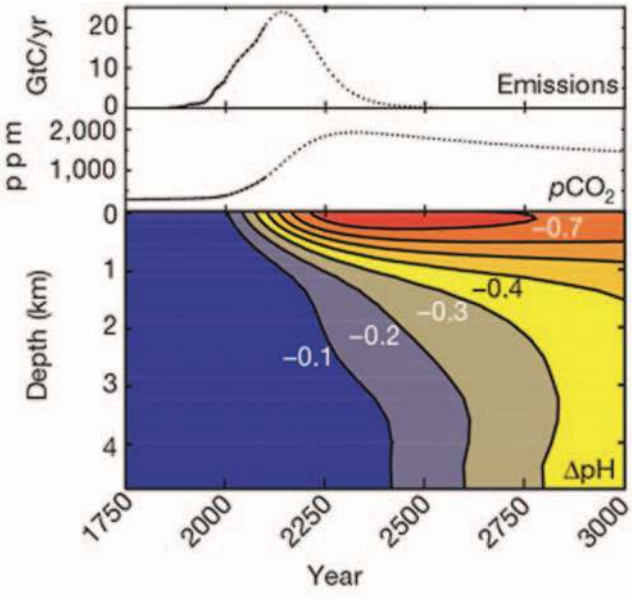

FIGURE 2 Model simulations of long-term changes in ocean pH, averaged horizontally, as a result of the CO_2 emissions shown in the top panel. pCO_2 is the atmospheric concentration of CO_2. REPRINTED FROM CALDEIRA AND WICKETT (2003), WITH PERMISSION FROM MACMILLAN PUBLISHERS LTD.

CAPACITY

Oceans occupy more than 70% of the Earth's surface and have an average depth of about 3.8 km. Considering the saturation concentration of CO_2 in seawater, this storage capacity is orders of magnitude greater than the capacity needed to absorb the CO_2 produced by burning all of the world's fossil fuel resources, equivalent to an estimated 5000 to 10,000 Gt C. However, a more realistic capacity estimate requires understanding ocean biogeochemistry and the expected environmental impact.

CO_2 exists in seawater in various forms as part of the carbonate system:

$$CO_2(aq) + H_2O \leftrightarrow H_2CO_3(aq) \leftrightarrow H^+ + HCO_3^- \leftrightarrow 2H^+ + CO_3^{2-} \quad (1)$$

The relative proportions of these species are defined by the pH of the solution and by equilibrium relationships. Dissolving additional CO_2 increases production of hydrogen ions (decreasing pH), but the change is buffered by conversion of carbonate into bicarbonate. Thus, the principal reactions for CO_2 dissolution in seawater are as follows:

$$CO_2 + H_2O + CO_3^{2-} \rightarrow 2HCO_3^- \quad (2)$$

$$CO_2 + H_2O \rightarrow H^+ + HCO_3^- \quad (3)$$

Decreased pH is one of the principal environmental impacts threatening marine organisms; the other is the concentration of CO_2 itself. Near the injection point, changes in pH and CO_2 concentration would be greatest, so injection schemes would have lowest impact if dilution is maximized. Far from the injection point, as CO_2 becomes widely distributed in the ocean, its impact would be similar to that of anthropogenic CO_2 absorbed from the atmosphere. Adding about 2000 Gt CO_2 to the ocean would reduce the *average* ocean pH by about 0.1 units, similar to the change already observed in the *surface* ocean. Adding about 5600 Gt CO_2 (about 200 years of current emissions) would decrease the average ocean pH by about 0.3 units (IPCC 2005).

The impact of such changes is not well known. However, one can examine spatial and temporal variations in ocean pH to understand how much change might be tolerated. The pH variability within latitudinal bands in each of the three major oceans (Pacific, Atlantic, Indian) during the 1990s was roughly 0.1 unit (IPCC 2005). If a change of 0.1 unit is assumed as a threshold tolerance and if the CO_2 is stored in the bottom half of the ocean (to maximize retention), approximately 1000 Gt CO_2 could be stored, enough to stabilize atmospheric concentrations at 500 ppm over the next 50 years, assuming energy consumption follows current trends and no other mitigation measures are put into place (Pacala and Socolow 2004). It should be realized that over the long term (millennia), the change in whole-ocean pH would ultimately be the same, whether CO_2 is released into the atmosphere or injected into the deep ocean, because thermodynamics drives the system to equilibrium. However, in the shorter term (several centuries), injecting into the deep ocean, below 1000 m depth, would limit pH drop in the near-surface, where marine biota are most plentiful, thus decreasing the adverse impact in the surface ocean.

INJECTION METHODS

Injection was first proposed by the Italian physicist Cesare Marchetti, who suggested dissolving CO_2 into the outflow from the Mediterranean Sea. Because this water is saltier than average seawater, the higher density would cause the CO_2 to sink into the depths of the Atlantic Ocean (Marchetti 1977). As illustrated in FIGURE 3, a number of options have been considered since then, including introducing the CO_2 as a rising or sinking plume, dispersing it from a moving ship, and creating a lake on the deep seafloor.

Before describing these methods in more detail, we first provide some background about the CO_2–seawater system. FIGURE 4 shows a simple phase diagram for CO_2 in seawater. At typical ocean pressure and temperature, pure CO_2 is in gas form above a depth of 400–500 m and in liquid form below. At a depth of 1000 m, liquid CO_2 is about 6% less dense than seawater. Because liquid CO_2 is more compressible than seawater, at a depth of 3000 m its density is similar to that of seawater. Thus liquid CO_2 would be positively buoyant and rise if it were injected above 3000 m, but it would sink if injected deeper. Below about 400 m depth, if the concentration of dissolved CO_2 is high enough, hydrate phases form. CO_2 hydrate, whose composition is given by $CO_2 \cdot nH_2O$ ($n \approx 5.75$), is a solid in which each CO_2 molecule sits in a cage-like structure of water molecules held together by hydrogen bonds. Unlike methane hydrates, which have a similar structure but are positively buoyant (Ruppel 2007), pure CO_2 hydrates are about 10% denser than seawater. Unless the surrounding water is saturated with CO_2, the hydrate is unstable, but it dissolves more slowly into seawater than does liquid CO_2.

Methods by which CO_2 is dissolved directly into seawater have received the most attention. The easiest scenario is to discharge it as a buoyant liquid, forming a rising droplet plume (Alendal and Drange 2001; Sato and Sato 2002). The required technology is available now to inject CO_2 from a manifold lying on the seafloor. Effective sequestration could be achieved by locating the manifold below the natural

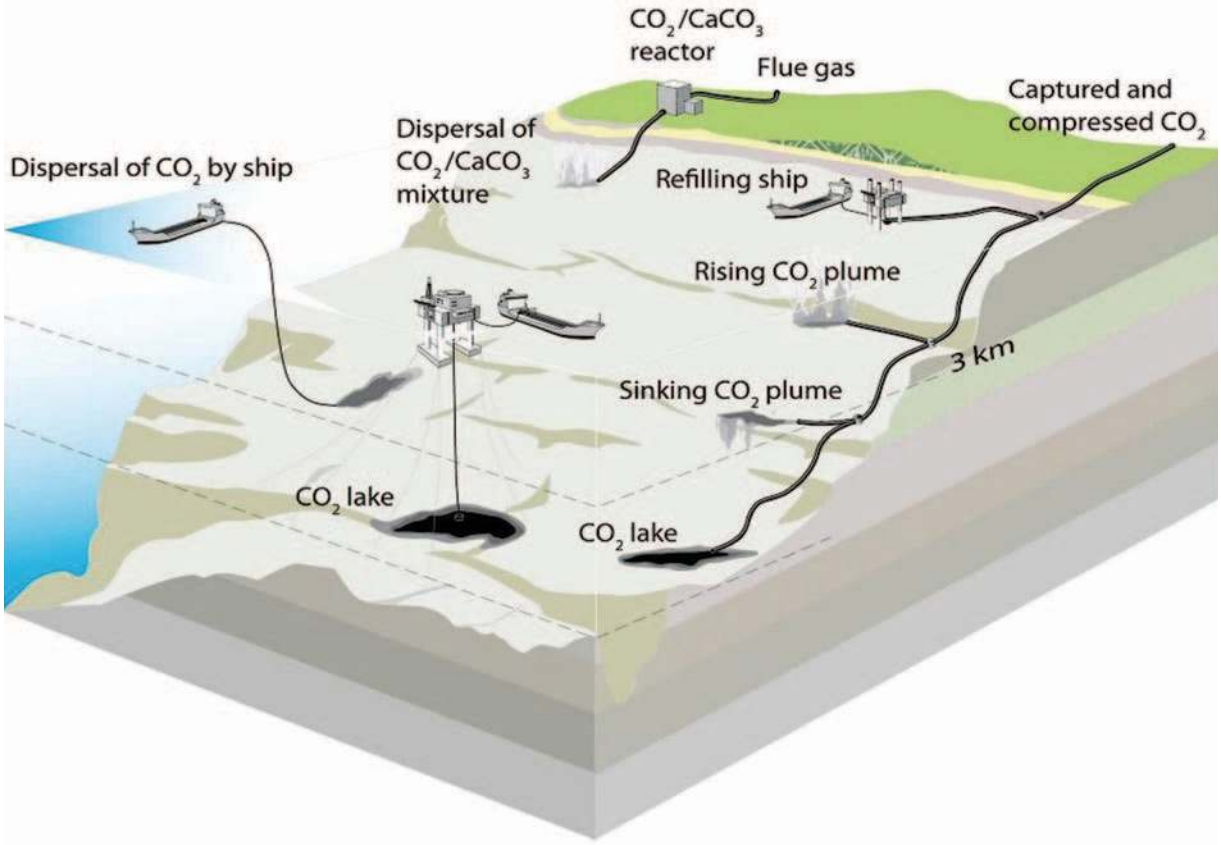

Figure 3 Strategies for ocean carbon sequestration. Reprinted from Figure TS-9: Special Report on Carbon Dioxide Capture and Storage (IPCC 2005), with permission from the Intergovernmental Panel on Climate Change

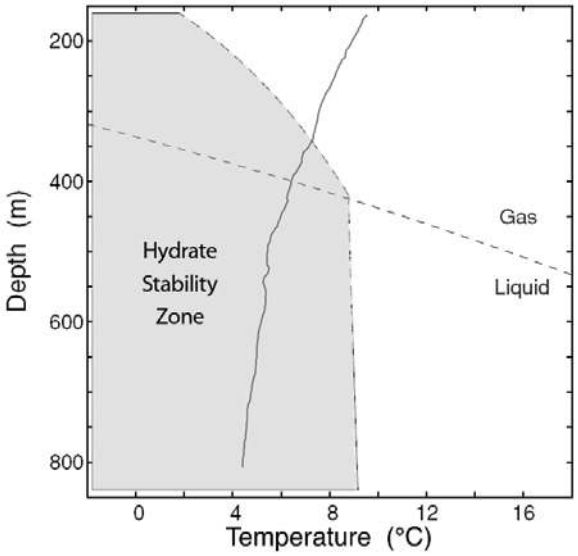

Figure 4 CO_2 phase diagram. Pressure is defined by water depth. The solid line indicates a temperature profile measured in Monterey Bay, California, USA. Above the dashed line, CO_2 in equilibrium with seawater is a gas, whereas below the line, it is a liquid. At sufficiently low temperature and high pressure, CO_2 hydrates form (grey region). Reprinted from Brewer et al. (2004; Figure 1), with permission from the author and Springer Science and Business Media

thermocline (the depth at which vertical temperature gradients in the ocean are strongest), and adequate dilution could be achieved by making the manifold sufficiently long. Even better dilution could be achieved by releasing CO_2 droplets from a ship, where motion provides additional dispersal (Ozaki et al. 2001). Although the delivery methods are different, the resulting plumes would be similar: each would yield a vertical band of CO_2-enriched seawater over a predetermined horizontal region.

Another dissolution option is to inject liquid CO_2 into a vessel where it can react at a controlled rate with seawater to form hydrates. While 100% reaction efficiency is difficult to achieve, laboratory and field experiments indicate that CO_2 sinks with as little as about 15–25% reaction efficiency (Tsouris et al. 2007). Instability leads to dissolution and dispersion during descent. The hydrate reactor could be towed from a moving ship, promoting additional dilution, or attached to a fixed platform, where the large concentration of dense particles and the increased seawater density caused by hydrate dissolution would create a sinking plume (Wannamaker and Adams 2006).

Dissolving high concentrations of CO_2 into seawater and then releasing the solution at the seafloor is another option (Haugan and Drange 1992). Enrichment with CO_2 causes only a slight density increase, but it is sufficient to promote sinking, especially within a submarine canyon. The environmental impact is higher, because the plume is more concentrated and it would come into direct contact with the seafloor, home to an abundance of relatively immobile fauna, bacteria, and algae. Alternatively, creating a CO_2 lake on the seafloor minimizes leakage to the atmosphere and exposure to biota (Ohsumi 1995; Haugan and Alendal 2005). A CO_2 lake would exist partly in the form of solid hydrates, which would slow dispersion to the water column, increasing retention time. Producing a lake would require more advanced technology and perhaps cost more than other options, because the lake must be more than 3000 m below the water surface.

Retention could be increased further using the reaction of CO_2 with carbonate minerals. Anthropogenic CO_2 currently transported to the deep ocean will equilibrate with carbonate sediments over a period of about 6000 years (Archer et al. 1998). Technical means could be used to accelerate this reaction, increasing effectiveness and diminishing the environmental impact. Power plant gas could be dissolved in seawater (Eq. 2) and then reacted with crushed limestone, either at the power plant or at the point of release, thus buffering pH change (Caldeira and Rau 2000). Conversely, an emulsion of liquid CO_2 and water could be stabilized by fine particles of pulverized limestone; the emulsion would be sufficiently dense to sink, and pH would be partially buffered by the limestone (Golomb et al. 2007). Drawbacks to these approaches include the cost to mine, crush, and transport large quantities of carbonate rock.

EFFECTIVENESS

Since the time when the oceans and atmosphere formed, they have exchanged CO_2 constantly. Now, about 350 Gt are exchanged each year, with a net ocean uptake of about 8 Gt CO_2 (IPCC 2005). Because of this exchange, one can ask how long it would take before injected CO_2 leaks back to the atmosphere. Long-term experiments with directly injected CO_2 have never been carried out, so effectiveness must be estimated from observations of other oceanic tracers, such as radiocarbon (^{14}C), and from computer models of ocean circulation and chemistry.

As a result of anthropogenic input, the atmosphere and ocean are currently out of equilibrium, so most emitted CO_2 will ultimately end up in the ocean. The percentage of CO_2 permanently sequestered is defined by thermodynamics and depends on the atmospheric concentration (Table 1). At today's atmospheric level of ~380 ppm, nearly 80% of CO_2 emitted *either* to the atmosphere *or* to the ocean would become permanently stored in the ocean, while at a concentration of 750 ppm, 70% would be stored. Of course, even at equilibrium, CO_2 would continue to be exchanged between the atmosphere and the ocean, so the carbon in the ocean on any given day would not be exactly the same carbon present on the previous day, even though the total would be constant. The predictions in Table 1 include the possibility of increased carbon storage in the terrestrial biosphere, but do not consider natural or engineered dissolution of carbonate minerals. Over thousands of years, retention would increase somewhat as CO_2 reacts with ocean sediments.

Table 1 implies that, for CO_2 injected into the ocean today, the *net quantity stored* ranges from 100% (now) to about 70–80% as the atmosphere approaches equilibrium with the ocean. One can also define retention as the fraction of injected CO_2 that is retained without ever reaching the surface; this fraction ranges from 100% at the time of injection to zero at equilibrium. The exact time depends on the location and depth of the injection.

Table 1 CO_2 PREDICTED TO BE PERMANENTLY SEQUESTERED IN THE OCEAN AS A FUNCTION OF ATMOSPHERIC CONCENTRATION

Atmospheric CO_2 concentration (ppm)	CO_2 permanently sequestered (%)
350	80
450	77
550	74
650	72
750	70
1000	66

Based on data in IPCC (2005) and references therein

Several computer-modeling studies have investigated CO_2 retention time in the world's oceans. The most comprehensive summary is the Global Ocean Storage of Anthropogenic Carbon (GOSAC) intercomparison study of several ocean general circulation models (OGCM). Ten models simulated the fate over 500 years of CO_2 injected at seven locations and three depths (Orr 2004). Figure 5 shows the fraction of CO_2 retained as a function of time, averaged over the seven sites. Although there is substantial variability, all models indicate increased retention with injection depth, and most predict over 70% retention after 500 years for injection at 3000 m. Note that these calculations assume CO_2 is dispersed in the water column at the injection depth. Formation of a CO_2 lake or reaction with marine sediments could increase retention time.

The time required for injected carbon from the deep ocean to enter the atmosphere is roughly equal to the time required for carbon from the atmosphere to reach the deep ocean. This can be estimated from observations of ^{14}C. Correcting for mixing with waters from various sources (polar ice, rivers, other oceans), the age of North Pacific deep water is estimated to be between 700 and 1000 years, while other basins, such as the North Atlantic, have turnover times of 300 years or more. These estimates are consistent with OGCM output and collectively suggest retention times of 300 to 1000 years. It is important to stress that CO_2 leakage to the atmosphere would take place gradually, over large areas of the ocean surface. Thus, unlike sequestration in porous rock, it would not be possible to produce a sudden release that could lead to harmful CO_2 concentrations at the ocean or land surface.

LOCAL ENVIRONMENTAL IMPACT AND PUBLIC PERCEPTION

Environmental impact may be the most significant factor determining the acceptability of ocean storage, because the strategy is grounded on the notion that impact on the deep ocean would be significantly less than the impacts avoided by limiting emission to the atmosphere. Above, we discussed environmental impacts from the global perspective. Here, we focus on the injection point.

A number of studies have summarized the potential impact on a variety of organisms, including adult and developing fish, zooplankton, and benthic fauna (Kikkawa et al. 2003; Ishimatsu et al. 2004; Pörtner et al. 2004; Watanabe et al. 2006). Earlier studies focused on the lethal impact on coastal fauna exposed to strong acids such as HCl (Auerbach et al. 1997), but recent work has examined the impact on deep-water organisms when exposed to CO_2, including sublethal effects (Kurihara et al. 2004). Organisms experience respiratory stress (decreased pH limits oxygen binding and transport of respiratory proteins), acidosis (low pH disrupts acid/base balance), and metabolic depression (elevated CO_2 causes some animals to reach a state of torpor). Data show a number of trends: (1) H_2CO_3 generally causes greater stress on an organism than an equivalent change in pH produced by another acid; (2) there are large differences in tolerance among different species and among different life stages of the same species; and (3) the duration of stress, as well as the level of stress, are important. While some studies suggest that deep organisms would be less tolerant than surface organisms, other studies have shown the opposite. Likewise, some animals are able to avoid regions of high CO_2 concentration (Vetter and Smith 2005), while others are less able (Tamburri et al. 2000). Results generally imply

that lethal effects can be avoided by achieving high near-field dilution. However, more research is needed, especially at the community level (e.g. studies of reduced lifespan, reproduction effects, and tolerance to other stresses).

The viability of ocean storage as a greenhouse gas mitigation option hinges on social, political, and regulatory considerations. In view of public precaution toward the ocean, which is a common, global resource, the strategy will require that all parties (private, public, non-governmental organizations) be included in ongoing research and debate. But the difficulty in this approach is highlighted by the recent experience of an international research team whose aim was to assess ocean carbon sequestration, as encouraged by the United Nations Framework Convention on Climate Change. A major part of their activity would have been a field test with 5 tons of CO_2 released off the coast of Norway. The plan was to monitor the physical, chemical, and biological effects of the injected CO_2 over a period of about a week. However, lobbying from environmental groups caused the Norwegian minister of the environment to rescind the group's permit (Giles 2002). Such actions unfortunately prevent collection of data that are critical for policy makers to evaluate the prudence of full-scale implementation.

COSTS AND COMPARISON WITH OTHER STORAGE METHODS

The storage media most comparable to the ocean, in terms of size and cost, are depleted or partially depleted hydrocarbon reservoirs and saline aquifers (Friedmann 2007; Benson and Cole 2008). Ocean storage and use of these geological media both require that CO_2 be captured and then compressed and transported to an injection site. Summarizing a number of studies, IPCC (2005) estimates the cost (2002 basis) of capture and compression for a coal- or gas-fired power plant at US$20–95 per ton CO_2 net captured and the cost of transportation at US$1–10 per ton CO_2 transported. The cost of geological storage is estimated at US$0.5–10 per ton CO_2 net injected, while the cost of ocean storage is estimated at US$5–30 per ton CO_2, making ocean storage somewhat more expensive (more details in Rubin 2008 this issue).

The aim of geological sequestration is to permanently trap the CO_2 within well-defined regions, so that it cannot interact with terrestrial or oceanic ecosystems. Sometimes CO_2 can be used to enhance oil recovery or coalbed methane production. For these reasons, geological storage has been favored. In contrast, most ocean disposal schemes aim to minimize impact by diluting the CO_2 in the vastness of the ocean, and while it may be isolated from the atmosphere for centuries, approximately 20–30% of it will eventually leak back. The ocean storage option that promises the most permanence is mineral carbonation, but this is more expensive—IPCC (2005) estimates the cost at US$50–100 per ton CO_2. On the other hand, compared with deep underground storage, CO_2 dispersed in the ocean is relatively easy to monitor, and because it is dispersed, the CO_2 that eventually reaches the atmosphere will escape slowly.

In a method that is hybrid between ocean and geologic storage, CO_2 would be injected into marine sediments, deep offshore (House et al. 2006). Because of the relatively high pressure and low temperature in this environment, the CO_2 would be negatively buoyant, perhaps forming solid hydrates, thus minimizing leakage through the sediment–water interface. And any CO_2 that was eventually released to the ocean would be dispersed and diluted.

Another form of ocean sequestration is enhanced production of biomass. Fertilizing portions of the world's oceans with iron would stimulate phytoplankton growth. The phytoplankton would increase the rate of biological uptake of CO_2 from the surface water and the atmosphere, and a portion would be transported to the ocean depths when the plankton dies. Iron fertilization is relatively inexpensive, and the organisms do most of the capture and transport, making this process an attractive solution. However, the technique is considered risky because it relies on deliberate manipulation of an ecosystem, with uncertain effects. At least ten international field experiments have been conducted to examine the short-term effects of iron fertilization (Coale et al. 2004). Although these experiments have demonstrated a clear response over the short term, the long-term effectiveness and the potential for detrimental changes to marine ecosystems are uncertain.

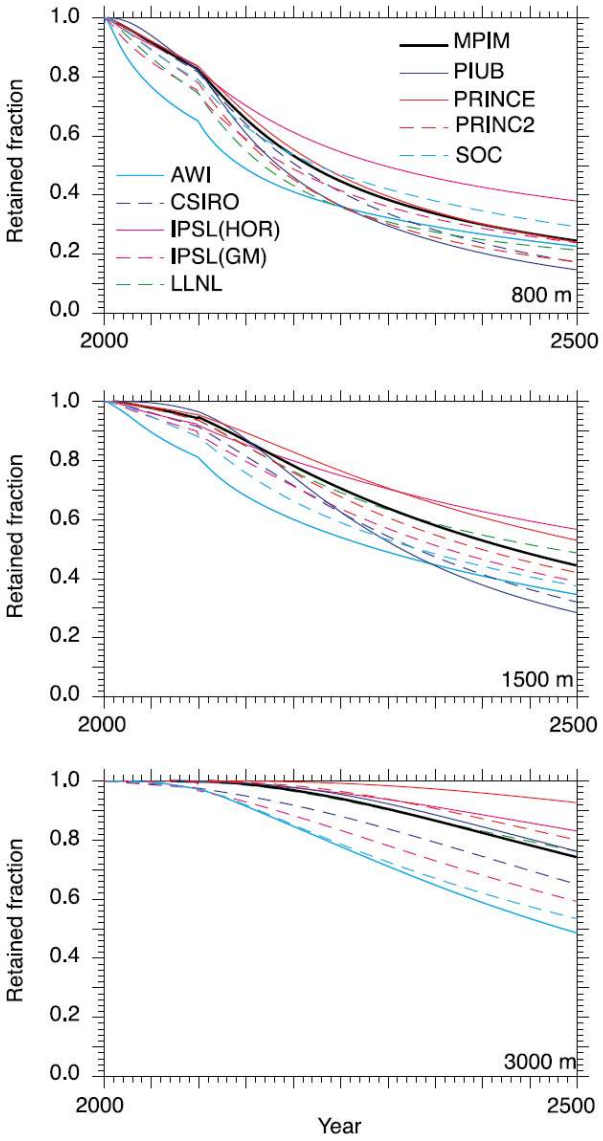

FIGURE 5 Comparison of ten model simulations, denoted by abbreviations (Orr 2004), showing as a function of time the amount of CO_2 that never reaches the ocean surface, for injection events at depths of 800 m, 1500 m, and 3000 m. Results are averaged over seven injection locations. Most of the CO_2 that does reach the surface remains in the ocean (TABLE 1), so the total retained is greater than shown here. REPRINTED FROM ORR (2004), WITH PERMISSION FROM IEA GREENHOUSE GAS R&D PROGRAMME

CONCLUSIONS

Ocean storage is one method to help mitigate global climate change. Compared to business as usual, ocean storage would reduce the peak CO_2 concentration and slow its rate of increase in both the atmosphere and ocean surface water. A number of injection schemes show promise for effective sequestration for several centuries, while diluting the concentration of CO_2 below levels of environmental concern. While such strategies appear promising, they require field verification. Reliable data are necessary before responsible decisions can be made about the safety of ocean storage. Because the ocean is common to all, public participation is essential. The ocean is vast but none the less finite, meaning ocean storage should be viewed as a potential interim solution, to be used while society prepares for its transition to more sustainable energy sources.

REFERENCES

Alendal G, Drange H (2001) Two-phase, near-field modeling of purposefully released CO_2 in the ocean. Journal of Geophysical Research 106(C1): 1085-1096

Archer DE, Kheshgi H, Maier-Reimer E (1998) Dynamics of fossil fuel CO_2 neutralization by marine $CaCO_3$. Global Biogeochemical Cycles 12: 259-276

Auerbach DI, Caulfield JA, Adams EE, Herzog HJ (1997) Impacts of ocean CO_2 disposal on marine life: I. A toxicological assessment integrating constant-concentration laboratory assay data with variable-concentration field exposure. Environmental Modeling and Assessment 2: 333-343

Benson SM, Cole DR (2008) CO_2 sequestration in deep sedimentary formations. Elements 4: 325-331

Brewer PG, Peltzer E, Aya I, Haugan P, Bellerby R, Yamane K, Kojima R, Walz P, Nakajima Y (2004) Small scale field study of an ocean CO_2 plume. Journal of Oceanography 60: 751-758

Broecker (2008) CO_2 capture and storage: Possibilities and perspectives. Elements 4: 295-297

Caldeira K, Rau GH (2000) Accelerating carbonate dissolution to sequester carbon dioxide in the ocean: Geochemical implications. Geophysical Research Letters 27: 225-228

Caldeira K, Wickett ME (2003) Anthropogenic carbon and ocean pH. Nature 425: 365

Coale KH and 47 coauthors (2004) Southern Ocean iron enrichment experiment: Carbon cycling in high- and low-Si waters. Science 304: 408-414

Friedmann SJ (2007) Geological carbon dioxide sequestration. Elements 3: 179-184

Giles J (2002) Norway sinks ocean carbon study. Nature 419: 6

Golomb D, Pennell S, Ryan D, Barry E, Swett P (2007) Ocean sequestration of carbon dioxide: Modeling the deep ocean release of a dense emulsion of liquid CO_2-in-water stabilized by pulverized limestone particles. Environmental Science & Technology 41: 4698-4704

Haugan PM, Drange H (1992) Sequestration of CO_2 in the deep ocean by shallow injection. Nature 357: 318-320

Haugan PM, Alendal G (2005) Turbulent diffusion and transport from a CO_2 lake in the deep ocean. Journal of Geophysical Research 110: C09S14, doi: 10.1029/2004JC002583

House KZ, Schrag DP, Harvey CF, Lackner KS (2006) Permanent carbon dioxide storage in deep-sea sediments. Proceedings of the National Academy of Sciences 103: 12291-12295

IPCC (2005) Special Report on Carbon Dioxide Capture and Storage. Prepared by Working Group III of the Intergovernmental Panel on Climate Change: Metz B, Davidson O, de Coninck HC, Loos M, Meyer LA (eds). Cambridge University Press, Cambridge, UK http://arch.rivm.nl/env/int/ipcc/pages_media/SRCCS-final/IPCCSpecialReportonCarbon dioxideCaptureand Storage.htm

Ishimatsu A, Kikkawa T, Hayashi M, Lee K-S, Kita J (2004) Effects of CO_2 on marine fish: Larvae and adults. Journal of Oceanography 60: 731-741

Kheshgi HS, Archer DE (2004) A nonlinear convolution model for the evasion of CO_2 injected into the deep ocean. Journal of Geophysical Research-Oceans 109: CO2007, doi: 10.1029/2002JC001489

Kikkawa T, Ishimatsu A, Kita J (2003) Acute CO_2 tolerance during the early developmental stages of four marine teleosts. Environmental Toxicology 18: 375-382

Kurihara H, Shimode S, Shirayama Y (2004) Sub-lethal effects of elevated concentrations of CO_2 on planktonic copepods and sea urchins. Journal of Oceanography 60: 743-750

Marchetti C (1977) On geoengineering and the CO_2 problem. Climatic Change 1: 59-68

Oelkers EH, Cole DR (2008) Carbon dioxide sequestration: A solution to a global problem. Elements 4: 305-310

Oelkers EH, Gislason SR, Matter J (2008) Mineral carbonation of carbon dioxide. Elements 4: 333-337

Ohsumi T (1995) CO_2 storage options in the deep sea. Marine Technology Society Journal 29: 58-66

Orr JC (2004) Modeling of Ocean Storage of CO_2—The GOSAC Study, Report PH4/37. International Energy Agency, Greenhouse Gas R&D Programme, 96 pp

Ozaki M, Minamiura J, Kitajima Y, Mizokami S, Takeuchi K, Hatakenaka K (2001) CO_2 ocean sequestration by moving ships. Journal of Marine Science and Technology 6: 51-58

Pacala S, Socolow R (2004) Stabilization wedges: Solving the climate problem for the next 50 years with current technologies. Science 305: 968-972

Pörtner HO, Langenbuch M, Reipschläger A (2004) Biological impact of elevated ocean CO_2 concentrations: lessons from animal physiology and Earth history. Journal of Oceanography 60: 705-718

Rubin (2008) CO_2 capture and transport. Elements 4: 311-317

Ruppel C (2007) Tapping methane hydrates for unconventional natural gas. Elements 3: 193-199

Sato T, Sato K (2002) Numerical prediction of the dilution process and its biological impacts in CO_2 ocean sequestration. Journal of Marine Science and Technology 6: 169-180

Tamburri MN, Peltzer ET, Friederich GE, Aya I, Yamane K, Brewer PG 2000 A field study of the effects of CO_2 ocean disposal on mobile deep-sea animals. Marine Chemistry 72: 95-101

Tsouris C and 10 coauthors (2007) Scaled-up ocean injection of CO_2–hydrate composite particles. Energy & Fuels 21: 3300-3309

Vetter EW, Smith CR (2005) Insights into the ecological effects of deep ocean CO_2 enrichment: the impacts of natural CO_2 venting at Loihi seamount on deep sea scavengers. Journal of Geophysical Research 110: C09S13, doi:10.1029/2004JC002617

Wannamaker EJ, Adams EE (2006) Modeling descending carbon dioxide injections in the ocean. Journal of Hydraulic Research 44: 324-337

Watanabe Y and 10 coauthors (2006) Lethality of increasing CO_2 levels on deep-sea copepods in the western North Pacific. Journal of Oceanography 62: 185-196